nature communications

Article

https://doi.org/10.1038/s41467-025-60698-1

cTAGE5 is essential for adipogenesis and adipose tissue development

Received: 27 June 2024

Accepted: 27 May 2025

Published online: 01 July 2025

Check for updates

Junwan Fan [1]✉, Tiantian Ma [2], Xiaoping Ren [1], Zhilin Chang [1], Dan Zhang [2], Yi Wang [1], Shiyao Cheng [1,3], Xin Qi [1], Kehui Liu [4], Yan Wang [5], Yaqing Wang [2], Zhiheng Xu [2,6]✉ & Wenyan He [1]✉

White adipocytes serve as primary energy reservoirs and their malfunction is linked to different metabolic disorders, yet the mechanisms underlying cellular specialization, a critical step during adipogenesis remain unknown. Here, we reveal the indispensable role of cutaneous T-cell lymphoma-associated antigen 5 (cTAGE5) in adipocyte differentiation and maturation. Conditional deletion of *cTAGE5* in adipocyte precursor cells (APCs), rather than mature adipocytes, results in progressive loss of white adipose tissue and death of mice. Mechanistically, *cTAGE5* deficiency in APCs disturbs pro-insulin receptor (IR) processing and impairs insulin signaling, accompanied by significant down-regulation of actin cytoskeleton related genes and defect in cytoskeleton remodeling, alongside enhanced expression of proteins associated with lipid catabolic process and lipolysis in adipocytes. Importantly, inhibitors targeting actin polymerization and lipolysis effectively restore adipocyte differentiation capacity in *cTAGE5*-deficient APCs. Collectively, our findings demonstrate that cTAGE5 plays pivotal roles in adipogenesis and adipose tissue development.

Adipocytes are the major constituent of white adipose tissue (WAT), which is essential for body growth, sustenance, and metabolic homeostasis[1,2]. WAT is critical for energy storage, as it consists of unilocular adipocytes with a large, single lipid droplet for storing energy, equipped with the enzymatic machinery for the synthesis and hydrolysis of triglyceride[3]. WAT also serves as endocrine tissue by secreting many adipokines, such as adiponectin and leptin[1,4]. WAT starts to form right after birth and advances during postnatal days in mice[5–7]. Inguinal WAT (iWAT) develops directly after birth, while epididymal WAT (eWAT) emerges at postnatal day[7], originating from a shared pool of platelet-derived growth factor receptor α positive (PDGFRA$^+$) precursor cells[5,8,9]. Lineage tracing experiments have shown that PDGFRA labels the precursor of all white adipocytes[10–12].

Accumulating data have shown that mature adipocytes are generated through the differentiation of adipocyte precursor cells (APCs) derived from stromal-vascular fractions (SVFs), termed adipogenesis[13,14]. This process is characterized by two consecutive phases: commitment and terminal differentiation[3]. Many combinations of surface markers have been applied in the identification of APCs during the adipogenesis process. For example, CD24, CD29, CD34, SCA-1 et al., combined with other excluding markers (CD31, CD45, Ter119), are able to enrich APCs and their developmental intermediate precursors. APCs contain two sequential cell populations defined by markers Lin$^-$CD29$^+$CD34$^+$SCA-1$^+$CD24$^+$ and Lin$^-$CD29$^+$CD34$^+$SCA-1$^+$CD24$^-$ ([8,10,15,16]). As part of the commitment process, adipocyte progenitor cells initially commit to preadipocytes

[1]China National Clinical Research Center for Neurological Diseases, Beijing Tiantan Hospital, Capital Medical University, Beijing, China. [2]State Key Laboratory of Molecular Developmental Biology, Institute of Genetics and Developmental Biology, Chinese Academy of Sciences, Beijing, China. [3]School of Public Health (Shenzhen), Sun Yat-sen University, Shenzhen, Guangdong, China. [4]State Key Laboratory of Organ Regeneration and Reconstruction, Institute of Zoology, Chinese Academy of Sciences, Beijing, China. [5]Clinical Biobank Center, Medical Innovation Research Division of Chinese, PLA General Hospital, Beijing, China. [6]The Second Affiliated Hospital, Zhejiang University School of Medicine, Hangzhou, Zhejiang, China. ✉e-mail: fanjunwan@ncrcnd.org.cn; zhxu@genetics.ac.cn; hewenyan77@ncrcnd.org.cn

and then undergo terminal adipocyte differentiation, ultimately acquiring the characteristics of mature adipocytes[17]. Adipocyte differentiation is controlled by a highly organized gene expression program that includes several master transcription factors, such as *Pparg*, *Cebpa*, and *Srebp1*[18,19]. Recent research indicates that adipocyte differentiation and maturation involve cytoskeleton remodeling and lipolysis to facilitate lipid storage in cytoplasmic lipid droplets[20–22]. Nevertheless, the mechanisms governing adipocyte differentiation during neonatal adipogenesis remain largely unclear.

Insulin receptor (IR) signaling has been recognized as an important regulator of glucose homeostasis and adipogenesis[23,24]. In adipose tissue, IR is essential for adipose tissue specification and lipid accumulation during WAT development and maintenance. However, it is less necessary for orchestrating WAT homeostasis in adults, likely due to the different regulatory mechanisms in developmental and adult WAT[25]. IR is synthesized in the endoplasmic reticulum (ER), processed in the golgi apparatus (Golgi), and then transferred to the plasma membrane[26–28]. Several studies have focused on IR endocytosis and recycling, yet the molecular mechanism underlying anterograde IR transport remains largely unknown.

Cutaneous T-cell lymphoma-associated antigen 5 (cTAGE5), also known as meningioma-expressed antigen 6 (MEA6), is widely expressed in multiple tissues and organs throughout embryonic development and serves as a key regulator of development and growth[29–31]. cTAGE5 has been shown to interact with COPII components and plays a crucial role in transporting cargoes, including very low-density lipoprotein (VLDL) from the ER to the Golgi and its secretion in the liver[32,33]. Meanwhile, its deficiency could alter the lipid composition in brain[29,34]. These studies indicate that cTAGE5 may play an important role in lipid metabolism. However, the function of cTAGE5 in adipogenesis and metabolic homeostasis and the underlying mechanisms have not been reported.

In this study, we generated and characterized a mouse model with conditional knockout of *cTAGE5* in APCs. We demonstrate that *cTAGE5* deficiency impedes adipocyte differentiation and causes a progressive loss of WAT mass, ultimately leading to the demise of mice. In addition, we provide evidence that *cTAGE5* deletion disturbs the processing of pro-insulin receptor (pro-IR), thereby disrupting the remodeling of the actin cytoskeleton while concurrently accelerating lipolysis during adipocyte differentiation.

Results

cTAGE5 deficiency in APCs leads to progressive loss of WAT mass

We performed phenome-wide association studies (PheWAS) based on data from the UK Biobank and association analysis of 704 young Chinese men and found that melanoma inhibitory activity 2 *(MIA2)*, another isoform of *cTAGE5*, is correlated with the human triglyceride (TG) and low-density lipoprotein (LDL) index (Supplementary Fig. 1a, b). This implies that cTAGE5 may also play a role in lipid metabolism.

We therefore inspected the expression of *cTAGE5* and found that it was expressed at similar levels in APCs, 3T3-L1 preadipocytes, and iWAT at different developmental stages (Supplementary Fig. 2a). To explore the biological function of cTAGE5 in adipose tissue, combined with previous reported that PDGFRA$^+$ cells represent adipocyte precursor cells (APCs) in vivo[10], we specifically deleted *cTAGE5* in APCs by crossing *cTAGE5*$^{flox/flox}$ mice with *Pdgfrα-Cre* transgenic mice. Littermates of *cTAGE5*$^{flox/flox}$;*Pdgfrα-Cre* and *cTAGE5*$^{flox/+}$ or *cTAGE5*$^{flox/flox}$ were denoted as conditional knockout (AP-cKO) and control (Ctrl) mice, respectively (Fig. 1a). We sorted the Lin$^-$CD29$^+$CD34$^+$SCA-1$^+$ PDGFRA$^+$ APCs from SVFs isolated from postnatal day 16 (P16) iWAT and observed that *cTAGE5* was specifically knocked out in primary PDGFRA$^+$ APCs (Supplementary Fig. 2b–d). According to previous reports, APCs were labeled by Lin$^-$CD29$^+$CD34$^+$SCA-1$^+$, and they were almost all PDGFRA positive, as shown in Supplementary Fig. 2b. Therefore, we sorted the Lin$^-$CD29$^+$CD34$^+$SCA-1$^+$ APCs population and confirmed the dramatically reduced *cTAGE5* expression in primary APCs and cultured SVFs, which are considered as preadipocytes or adipocyte-derived stem cells (Supplementary Fig. 2e and Fig. 1b, c). Furthermore, immunoblot analysis of isolated iWAT, eWAT, and brown adipose tissue (BAT) revealed the significantly reduced expression of cTAGE5 in AP-cKO mice, but not in the liver (Supplementary Fig. 2f), indicating that *cTAGE5* was effectively knocked out in adipose tissue.

cTAGE5 AP-cKO mice exhibited severe growth defects grossly (Fig. 1d). Their body weight decreased gradually after P8, and all died before P21 (Fig. 1e, f). To detect the effect of *cTAGE5* ablation on adipose tissue, we isolated iWAT, eWAT, and BAT from P8, P12, and P16 control and AP-cKO mice. The WAT mass of AP-cKO mice was dramatically decreased at P12 (47 ± 6.69 mg vs. 171 ± 25.74 mg) and P16 (iWAT: 53.07 ± 9.063 mg vs. 272.2 ± 21.52 mg; eWAT: 3.168 ± 0.607 mg vs. 28.8 ± 3.729 mg) (Fig. 1h, i). There was no difference at P8 (Fig. 1g). Moreover, the ratio of WAT to body weight in AP-cKO mice was also decreased compared to controls at P12 ($1.13 \pm 0.07\%$ vs. $2.21 \pm 0.19\%$) and P16 (iWAT: $1.09 \pm 0.12\%$ vs. $2.91 \pm 0.15\%$; eWAT: $0.07 \pm 0.01\%$ vs. $0.32 \pm 0.03\%$) (Fig. 1h, i). Interestingly, although the BAT mass was decreased at P12 and P16 AP-cKO mice, the ratio of BAT to body weight showed no change (Fig. 1h, i), indicating that *cTAGE5* deletion affects the development of WAT more significantly, leading to progressive reduction of WAT.

cTAGE5 ablation in APCs reduces the size of adipocytes in WAT and decreases lipid accumulation in BAT

To further investigate the effect of *cTAGE5* deletion on adipocytes, we performed histological analyses and observed that the size of adipocytes in iWAT was similar in P8 AP-cKO and control mice (Fig. 2a–c). However, iWAT of P12 and P16 AP-cKO mice contained a significantly higher frequency of small-sized adipocytes, concomitantly with dramatically less big-sized adipocytes. Specifically, the average size of adipocytes in AP-cKO mice decreased by approximately 50.2% at P12 and 82.1% at P16 (Supplementary Fig. 3a–c and Fig. 2h–j). Additionally, the accumulation of lipid droplets in AP-cKO BAT decreased at P8, P12, and P16 (Fig. 2d, k and Supplementary Fig. 3d), yet the mRNA levels of transcription factors associated with BAT function exhibited no difference (Supplementary Fig. 3e). Nonetheless, the structure of the liver was largely normal in P16 AP-cKO mice (Supplementary Fig. 3f), indicating the specific effect on white adipose tissue.

To inspect the effect of *cTAGE5* deletion on serum lipids, we examined the serum levels of TG, total cholesterol (TC), glycerol, and nonestesterified fatty acid (NEFA) at different postnatal days. Our findings revealed no significant alterations in lipid levels between the AP-cKO and control mice, except for elevated glycerol and NEFA levels in P8 AP-cKO mice (Fig. 2e–g, l–n and Supplementary Fig. 3g, h). Notably, the smaller size of adipocytes and the diminished mass of WAT in P16 female AP-cKO mice closely resembled those of males (Supplementary Fig. 4), suggesting no gender impact on the phenotype. The above results indicate that cTAGE5 plays a crucial role in adipose tissue development, and its deletion in APCs leads to a significant reduction in adipocyte size.

cTAGE5 deficiency in mature adipocytes does not significantly affect adipose tissue homeostasis

To verify whether cTAGE5 had any effect on mature adipocytes, we specifically deleted *cTAGE5* in mature adipocytes by crossing *cTAGE5*$^{flox/flox}$ mice with *Adiponectin (AD)-Cre* transgenic mice[27]. Diminished cTAGE5 expression in WAT and BAT but not liver was confirmed by western blotting in 8-week-old *cTAGE5*$^{flox/flox}$*; AD-Cre* (AD-cKO) mice (Supplementary Fig. 5a). Compared to the loss of body weight and WAT mass in AP-cKO mice, *cTAGE5* AD-cKO mice did not display any phenotypic traits in body weight, the WAT mass, and the ratio of WAT to body weight (Supplementary Fig. 5b, c). Histological analysis

 https://doi.org/10.1038/s41467-025-60698-1

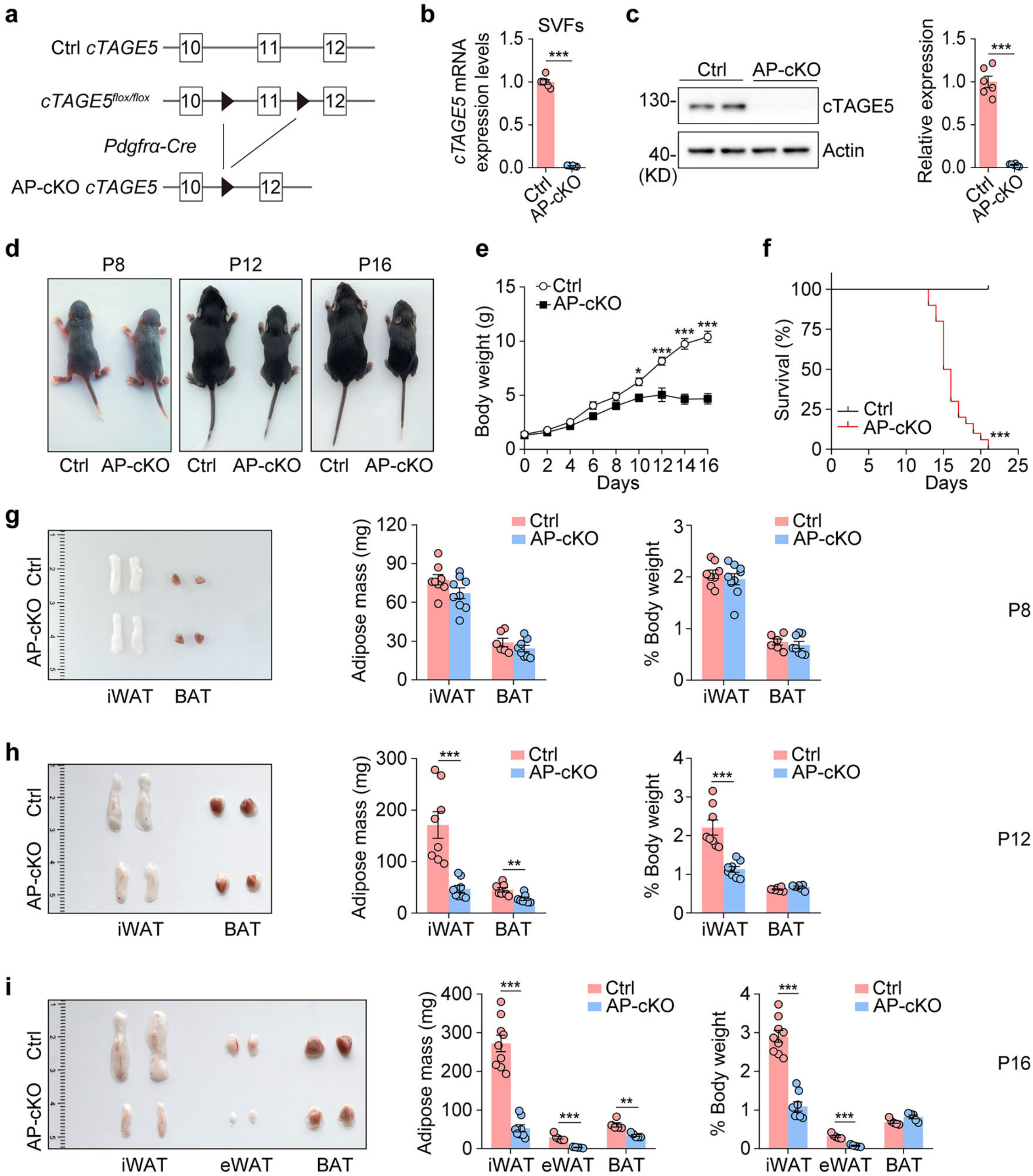

Fig. 1 | *cTAGE5* deficiency in APCs leads to progressive loss of WAT and death of mice. a Targeting strategy for APC-specific deletion of *cTAGE5*. Exons were indicated by numbers, and triangles represent LoxP sites. Ctrl: *cTAGE5*$^{flox/+}$ or *cTAGE5*$^{flox/flox}$; AP-cKO: *cTAGE5*$^{flox/flox}$;*Pdgfrα-Cre*. **b** Relative *cTAGE5* mRNA levels in cultured P16 SVFs detected by real-time PCR (Ctrl and AP-cKO, $n = 6$ biologically independent samples). **c** Western blotting analysis of cTAGE5 in cultured P16 SVFs and quantification by normalization to actin (Ctrl and AP-cKO, $n = 6$ biologically independent samples). **d** Representative images of mice at P8, P12, and P16. **e** Body weight from P0 to P16 (Ctrl, $n = 11, 7, 6, 7, 10, 6, 6, 6, 7$ biologically independent mice on 0, 2, 4, 6, 8, 10, 12, 14, 16 days respectively; AP-cKO, $n = 6, 6, 4, 6, 7, 6, 4, 5, 7$ biologically independent mice on 0, 2, 4, 6, 8, 10, 12, 14, 16 days respectively). **f** Postnatal survival curve (Ctrl and AP-cKO, $n = 50$ biologically independent mice). **g**, **h** iWAT and BAT depots isolated from P8 (**g**) and P12 (**h**) control and AP-cKO mice. Adipose mass and the ratio to body weight were shown at right (**g**, iWAT: Ctrl, $n = 8$ biologically independent mice; AP-cKO, $n = 9$ biologically independent mice; BAT: Ctrl, $n = 6$ biologically independent mice; AP-cKO, $n = 8$ biologically independent mice; **h** iWAT: Ctrl and AP-cKO, $n = 8$ biologically independent mice; BAT: Ctrl and AP-cKO, $n = 7$ biologically independent mice). **i** iWAT, eWAT, and BAT depots isolated from P16 control and AP-cKO mice. Adipose mass and the ratio to body weight were shown at right (iWAT: Ctrl, $n = 9$ biologically independent mice; AP-cKO, $n = 8$ biologically independent mice; eWAT: Ctrl and AP-cKO, $n = 5$ biologically independent mice; BAT: Ctrl and AP-cKO, $n = 5$ biologically independent mice). **b**, **c** Representative of three independent experiments. **e**, **g**–**i** Representative of four independent experiments. All data are mean ± s.e.m. $^{*}P < 0.05$, $^{**}P < 0.01$, and $^{***}P < 0.001$. Unpaired two-tailed Student's *t*-test (**b**, **c**, **h**, **i**) or two-way ANOVA followed by Bonferroni post hoc test (**e**) or log-rank test (**f**). Source data with exact *P*-value are provided as a Source Data file.

showed that AD-cKO mice contained a slightly higher frequency of big-size adipocytes, with no significant change in the average adipocyte size of eWAT (Supplementary Fig. 5d, e). Glucose homeostasis was assessed in 8-week-old control and AD-cKO mice, and no between-group differences were observed in the glucose tolerance and insulin tolerance tests (Supplementary Fig. 5f, g). Additionally, there were no differences in the serum TG and TC levels between control and AD-cKO mice (Supplementary Fig. 5h, i). These results indicate that *cTAGE5*

https://doi.org/10.1038/s41467-025-60698-1

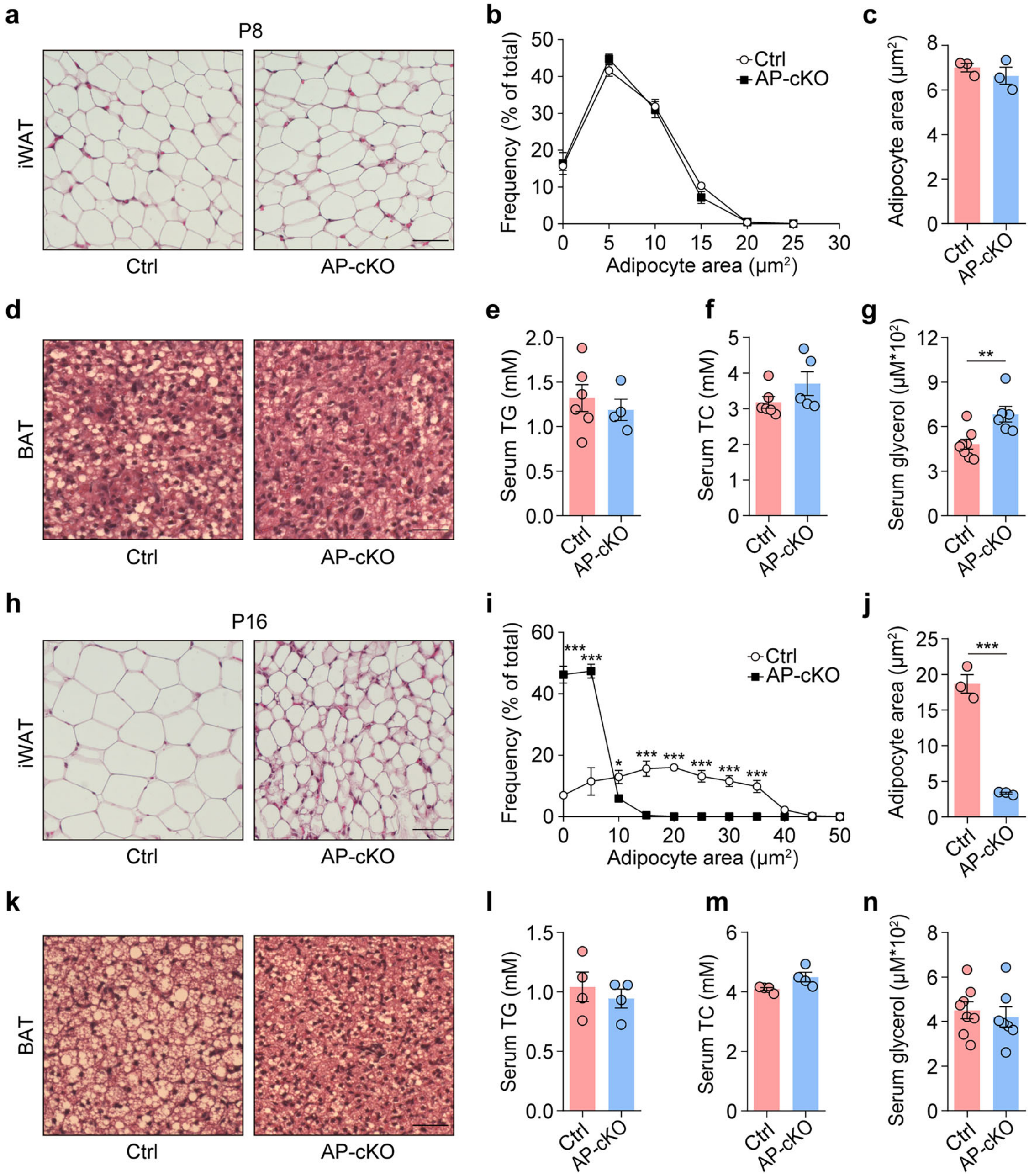

Fig. 2 | *cTAGE5* ablation in APCs reduces the size of adipocytes in WAT and decreases lipid accumulation in BAT. a H&E staining of P8 iWAT sections (Ctrl and AP-cKO, $n = 3$ biologically independent samples). Scale bar, 5 μm. **b**, **c** Adipocyte area distribution (**b**) and average adipocyte area (**c**) from P8 iWAT sections were calculated using Adiposoft software (Ctrl and AP-cKO, $n = 3$ biologically independent samples). **d** H&E staining of P8 BAT sections (Ctrl and AP-cKO, $n = 3$ biologically independent samples). Scale bar, 50 μm. **e**–**g** Levels of TG, TC, and glycerol in serum from P8 control and AP-cKO mice (Ctrl, $n = 6$, 6, 8 biologically independent mice in (**e**–**g**), respectively; AP-cKO, $n = 4$, 5, 6 biologically independent mice in (**e**–**g**), respectively). **h** H&E staining of P16 iWAT sections (Ctrl and AP-cKO, $n = 3$ biologically independent samples). Scale bar, 5 μm. **i**, **j** Adipocyte area distribution (**i**) and average adipocyte area (**j**) from P16 iWAT sections were calculated as in (**b**, **c**) (Ctrl and AP-cKO, $n = 3$ biologically independent samples). **k** H&E staining of P16 BAT sections (Ctrl and AP-cKO, $n = 3$ biologically independent samples). Scale bar, 50 μm. **l**–**n** Levels of TG, TC, and glycerol in serum from P16 control and AP-cKO mice (Ctrl, $n = 4$, 4, 8 biologically independent mice in (**l**–**n**) respectively; AP-cKO, $n = 4$, 4, 7 biologically independent mice in (**l**–**n**), respectively). **a**–**n** Representative of three independent experiments. All data are mean ± s.e.m. $^{*}P < 0.05$, $^{**}P < 0.01$, and $^{***}P < 0.001$. Unpaired two-tailed Student's *t*-test (**g**, **j**) or two-way ANOVA followed by Bonferroni post hoc test (**i**). Source data with exact *P*-value are provided as a Source Data file.

deletion in mature adipocytes does not affect adipose tissue or metabolic function significantly.

cTAGE5 deletion in APCs impedes adipocyte differentiation

APCs typically undergo proliferation and differentiation into mature adipocytes. To determine how *cTAGE5* deletion in APCs leads to severe WAT reduction, we isolated and labeled APCs based on established cell surface markers ($Lin^{-}CD29^{+}CD34^{+}SCA\text{-}1^{+}$) from iWAT of P8 control and AP-cKO mice (Fig. 3a). Flow cytometric analysis showed a significant increase in both the percentage and the absolute number of APCs in AP-cKO iWAT (Fig. 3b, c), leading to our speculation of accelerated proliferation and/or reduced differentiation of APCs. We then inspected the cell cycle of P8 APCs by staining with Ki67 and observed a

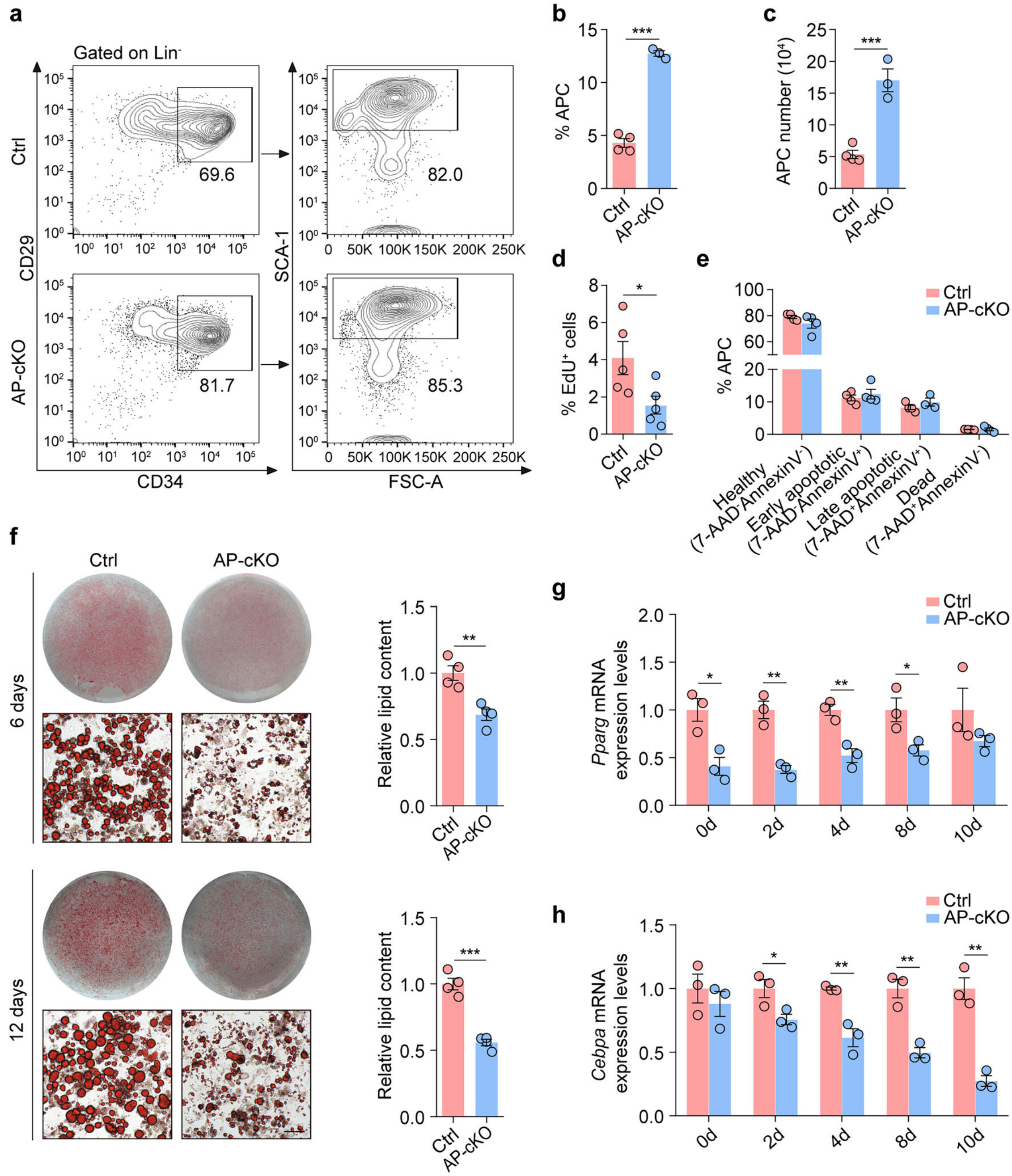

Fig. 3 | *cTAGE5* deletion in APCs impedes adipocyte differentiation. **a** Representative flow cytometric analysis showing the percentage of APCs ($Lin^-CD29^+CD34^+SCA\text{-}1^+$) isolated from P8 iWAT of control and AP-cKO mice. **b**, **c** Percentage (**b**) and absolute number (**c**) of APCs isolated from P8 iWAT (Ctrl, $n = 4$ biologically independent samples; AP-cKO, $n = 3$ biologically independent samples). **d** EdU incorporation in APCs after injecting for 3 days. The percentage of EdU-positive cells was measured (Ctrl and AP-cKO, $n = 5$ biologically independent samples). **e** APCs isolated from P8 iWAT were stained with Annexin V and 7-AAD and analyzed by flow cytometry. The percentage of apoptotic cells in APCs was measured (Ctrl and AP-cKO, $n = 4$ biologically independent samples). **f** Oil Red O staining and quantification of P8 SVFs after inducing adipocyte differentiation for 6 and 12 days (Ctrl and AP-cKO, $n = 4$ biologically independent samples). Scale bars, 50 µm. **g**, **h** mRNA expression levels of *Pparg* (**g**) and *Cebpa* (**h**) during adipocyte differentiation were detected (Ctrl and AP-cKO, $n = 3$ biologically independent samples). **a**–**h** Representative of three independent experiments. All data are mean ± s.e.m. $^*P < 0.05$, $^{**}P < 0.01$, and $^{***}P < 0.001$. Unpaired two-tailed Student's *t*-test (**b**–**d**, **f**–**h**). Source data with exact *P*-value are provided as a Source Data file.

decrease in G0 phase cells (9.38 ± 0.37% vs. 17.75 ± 1.66%), but an increase in G1 phase cells (86.4 ± 0.75% vs. 76.33 ± 0.84%) in AP-cKO APCs (Supplementary Fig. 6a). For further confirmation, we measured 5-ethynyl-2′-deoxyuridine (EdU) incorporation in APCs by injecting 100 mg/kg EdU intraperitoneally for 3 days, and found a significantly reduction of EdU-positive cells (1.56 ± 0.48% vs. 4.09 ± 0.89%) in AP-cKO APCs (Fig. 3d). In addition, *cTAGE5* deletion does not affect apoptosis of APCs as shown by Annexin V and 7-AAD staining (Fig. 3e). These results indicate that *cTAGE5* deletion disturbs the proliferation of APCs in P8 mice.

To verify whether the increased number of APCs in AP-cKO mice was due to the impediment of APCs differentiation, we isolated and cultured SVFs from P8 and P16 iWAT. After induction with adipogenic stimuli by 6 and 12 days, we found that the SVFs from AP-cKO mice had a significantly reduced ability to undergo adipocyte differentiation based on the accumulation of cells with no lipid droplets or with

https://doi.org/10.1038/s41467-025-60698-1

smaller-sized lipid droplets, and a significant decrease in total lipid accumulation as shown by quantification of Oil Red O staining (Fig. 3f and Supplementary Fig. 6b). Accordingly, the mRNA levels of adipogenic transcription factors *Pparg* and *Cebpa* were significantly lower during adipocyte differentiation in P8 AP-cKO SVFs (Fig. 3g, h). Interestingly, we observed a similar trend in *cTAGE5* expression levels to *Pparg*, *Cebpa*, and *Plin1* during adipocyte differentiation (Supplementary Fig. 6c–f).

To further confirm the function of cTAGE5 in adipocyte differentiation, we knocked down cTAGE5 expression in 3T3-L1 preadipocytes (3T3-L1-KD) and human adipose-derived stem cells (hADSC-KD) via lentivirus-mediated short hairpin RNA (shRNA). Reduced expression of cTAGE5 was confirmed by both real-time PCR analysis and western blotting (Supplementary Figs. 7a, b and 8a, b). Since the viability of 3T3-L1-KD cells was not altered (Supplementary Fig. 7c), we then treated the control and 3T3-L1-KD/hADSC-KD cells with adipogenic stimuli and observed that the adipogenic ability was severely inhibited in 3T3-L1-KD/hADSC-KD cells, recapitulating that in *cTAGE5* AP-cKO SVFs. Oil Red O staining showed that the size and number of lipid droplets and total lipid accumulation were also significantly reduced in 3T3-L1-KD/hADSC-KD cells (Supplementary Figs. 7d, 8c), as well as the expression of adipogenic genes (Supplementary Figs. 7e, f and 8d, e). However, SVFs isolated from *cTAGE5* AD-cKO mice exhibited similar adipogenic differentiation ability compared with controls (Supplementary Fig. 9a, b). Taken together, these results demonstrated that *cTAGE5* deletion in APCs but not in mature adipocytes severely impeded WAT formation mainly due to the disturbance of APCs differentiation and adipogenesis.

cTAGE5 deletion in APCs disturbs actin cytoskeleton remodeling during adipocyte differentiation

To elucidate how *cTAGE5* deletion affects adipocyte differentiation, we isolated and sorted out APCs from the iWAT of P8 control and AP-cKO mice for bulk RNA sequencing (RNA-seq). This identified 528 significant differentially expressed genes (DEGs) (fold change >1.5 and adjusted $P < 0.05$), including 227 upregulated and 301 downregulated genes (Fig. 4a). Furthermore, using gene set enrichment analysis (GSEA), we found that genes involved in the regulation of actin cytoskeleton and cell cycle-related biological processes were significantly downregulated in AP-cKO APCs compared to controls (Fig. 4b, c), which were verified by real-time PCR analysis (Fig. 4d, e).

Since actin cytoskeleton remodeling is a prerequisite for adipocyte differentiation[21], we speculated that cTAGE5 might participate in actin cytoskeleton remodeling, thereby affecting the process of adipocyte differentiation. To test this hypothesis, we inspected the dynamics of the actin cytoskeleton during adipocyte differentiation by staining actin with FITC-labeled phalloidin. In undifferentiated cells (0 day), actin filaments were well organized as regular stress fibers across the cell body in both control and AP-cKO SVFs. After 4 days of adipogenic stimuli, the actin cytoskeleton of control SVFs was distributed to the cortical region near the plasma membrane, whereas the actin fiber network in AP-cKO SVFs was still distributed across the cell body (Fig. 4f), demonstrating that *cTAGE5* deletion disturbs the remodeling of the actin cytoskeleton. However, the morphology of microtubules was similar between control and AP-cKO SVFs at both 0 and 4 days of adipocyte differentiation (Supplementary Fig. 10a), suggesting that *cTAGE5* deletion specifically affects actin cytoskeleton remodeling.

To clarify whether the defective actin cytoskeleton remodeling caused by loss of *cTAGE5* is a consequence or cause of the APC differentiation defect, we treated control and AP-cKO SVFs with Latrunculin B (LatB), an inhibitor of actin polymerization, to promote actin cytoskeleton remodeling. At day 10 after LatB treatment, Oil Red O staining results showed that lipid accumulation and total lipid content increased significantly in AP-cKO SVFs compared to vehicle (Veh, DMSO) treated cells (Fig. 4g). Of note, another actin polymerization inhibitor, cytochalasin D (CytoD), could also rescue the impeded adipocyte differentiation in AP-cKO SVFs. However, the tubulin polymerization inhibitor nocodazole (Noco) had no effect (Supplementary Fig. 10b).

Recent studies showed that MYL9, a regulatory subunit of non-muscle motor protein myosin II (NMII), binds to actin filaments to control cytoskeletal dynamics[35,36]. We found that the expression of myosin light chain 9 (MYL9) was significantly decreased in AP-cKO APCs and 3T3-L1-KD cells compared to their respective controls (Fig. 4d and Supplementary Fig. 10c–e). Moreover, the expression of *Myl9* was also decreased during adipocyte differentiation in 3T3-L1-KD cells (Supplementary Fig. 10f). We thereby stably knocked down MYL9 expression in 3T3-L1 cells and stimulated adipogenic differentiation. Oil Red O staining results showed that total lipid accumulation decreased significantly (Supplementary Fig. 10g). This further verified the important role of actin cytoskeleton remodeling during adipocyte differentiation. Collectively, the above results indicate that cTAGE5 functions in adipocyte differentiation, possibly through the remodeling of the actin cytoskeleton.

cTAGE5 deletion in APCs enhances lipolysis in WAT adipocytes

TG synthesis and lipolysis maintain a dynamic balance during adipocyte differentiation[37]. Since the levels of serum glycerol and NEFA increase in P8 AP-cKO mice and the amounts of WAT reduce progressively, we postulated that *cTAGE5* deletion resulted in increased lipolysis. To test this, we isolated iWAT from P8 control and AP-cKO mice for mass spectrometry analysis. Gene Ontology (GO) analysis of differentially expressed proteins showed that proteins related to lipid catabolic processes were significantly upregulated in AP-cKO iWAT (Fig. 5a). To gain insight into the activation of the lipolytic pathway in the absence of *cTAGE5*, we inspected the expression of key lipolytic enzymes (*Atgl*, *Hsl*, *Mgl*) in P8, P16 iWAT, and in differentiated SVFs by real-time PCR, and detected their significant upregulation (Fig. 5b–d and Supplementary Fig. 11a–c). Furthermore, we performed ex vivo lipolysis experiments and found a significantly higher level of released glycerol under stimulated conditions in AP-cKO iWAT than in controls when normalized to the weight of fat pads (Fig. 5e and Supplementary Fig. 11d). Through transmission electron microscopy (TEM), we observed many small lipid droplets in iWAT adipocytes from P16 AP-cKO mice, whereas they were almost absent in the controls (Fig. 5f). This confirmed the enhanced lipolysis in AP-cKO mice.

Meanwhile, through depictions of the linkages between proteins and relevant biological concepts, we observed that Patatin-like phospholipase domain-containing protein 2 (PNPLA2), also named adipose triglyceride lipase (ATGL), may play an important role in these pathways (Supplementary Fig. 11e). Western blotting results verified that ATGL levels were increased by 65% in iWAT from P8 AP-cKO mice, consistent with the mass spectrometry analysis (Fig. 5g). We then examined the effect of ATGL inhibitor (atglistatin, Atgli) in AP-cKO SVFs. Primary SVFs isolated from P8 iWAT of control and AP-cKO mice were treated with Veh (DMSO) and 5 μM Atgli at 3 days after adipogenic cocktail treatment. After 10 days' treatment, Atgli enhanced lipid accumulation and total lipid content as determined by Oil Red O staining (Fig. 5h and Supplementary Fig. 11f). Intriguingly, in the presence of LatB or CytoD, addition of the Atgli to AP-cKO SVFs could further enhance lipid accumulation to a level similar to that of controls (Fig. 5h and Supplementary Fig. 11f). We went on to inject 200 μM/kg Atgli intraperitoneally into control and AP-cKO mice at P8, P11 and P14, and observed that Atgli extended the lifespan of 50% of AP-cKO mice by 2–3 days (Fig. 5i). Additionally, the injection of Atgli increased the body weight of AP-cKO mice by approximately 18.2% (Fig. 5j), yet the ratio of iWAT to body weight remained unchanged (Fig. 5k). The above results indicate that actin cytoskeleton remodeling and lipolysis pathways may jointly contribute to *cTAGE5* deficiency-induced white adipose tissue atrophy.

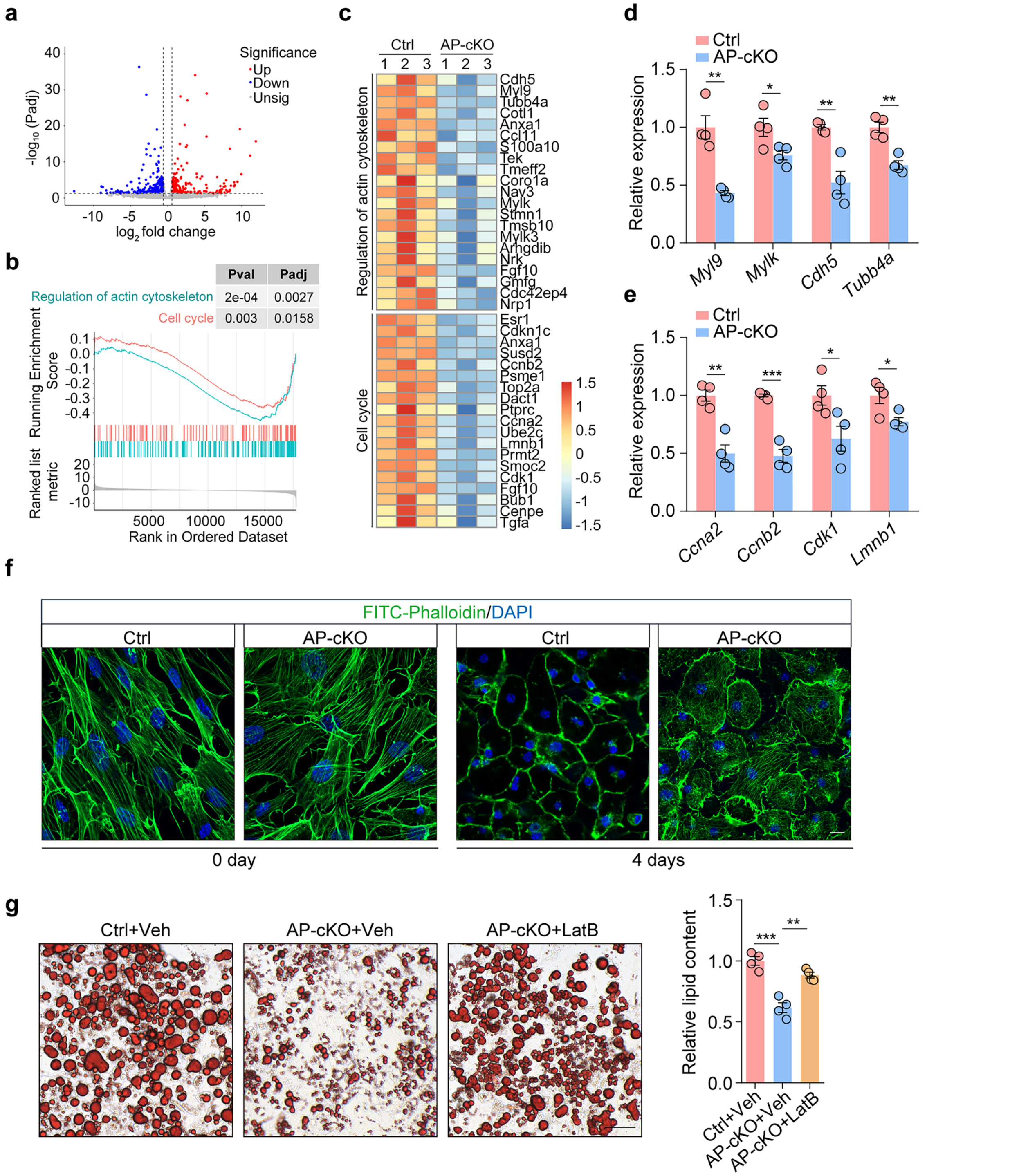

Fig. 4 | *cTAGE5* deletion in APCs disturbs actin cytoskeleton remodeling during adipocyte differentiation. a, **b** Volcano analysis of the upregulated and downregulated genes in APCs from P8 control and AP-cKO mice (**a**) and running enrichment score of GSEA comparison (**b**). Statistical significance (adjusted P-value < 0.05) was determined by the two-tailed Wald test for differential expression analyses and the phenotypic-based permutation test for GSEA. The Benjamini–Hochberg method was used to calculate adjusted P-values for multiple hypothesis testing. **c** Heatmap of leading genes' expression from GSEA. Actin cytoskeleton and cell cycle-related genes were downregulated in P8 AP-cKO APCs. **d**, **e** Relative mRNA expression of indicated genes in primary APCs isolated from P8 iWAT (Ctrl and AP-cKO, $n = 4$ biologically independent samples). **f** FITC-labeled phalloidin staining of P8 SVFs after inducing adipocyte differentiation for 0 and 4 days (Ctrl and AP-cKO, $n = 4$ biologically independent samples). Scale bars, 10 µm. **g** Primary P8 SVFs treated with Vehicle (Veh, DMSO) or 1 µM Latrunculin B (LatB) for 2 hours at 0 and 3 days after adipogenic cocktail treatment. Oil Red O staining and quantification of SVFs after inducing adipocyte differentiation for 10 days (Ctrl and AP-cKO, $n = 4$ biologically independent samples). Scale bars, 50 µm. **d**–**g** Representative of three independent experiments. All data are mean ± s.e.m. $^{*}P < 0.05$, $^{**}P < 0.01$, and $^{***}P < 0.001$. Unpaired two-tailed Student's t-test (**d**, **e**) or one-way ANOVA followed by Bonferroni post hoc test (**g**). Source data with exact P-value are provided as a Source Data file.

https://doi.org/10.1038/s41467-025-60698-1

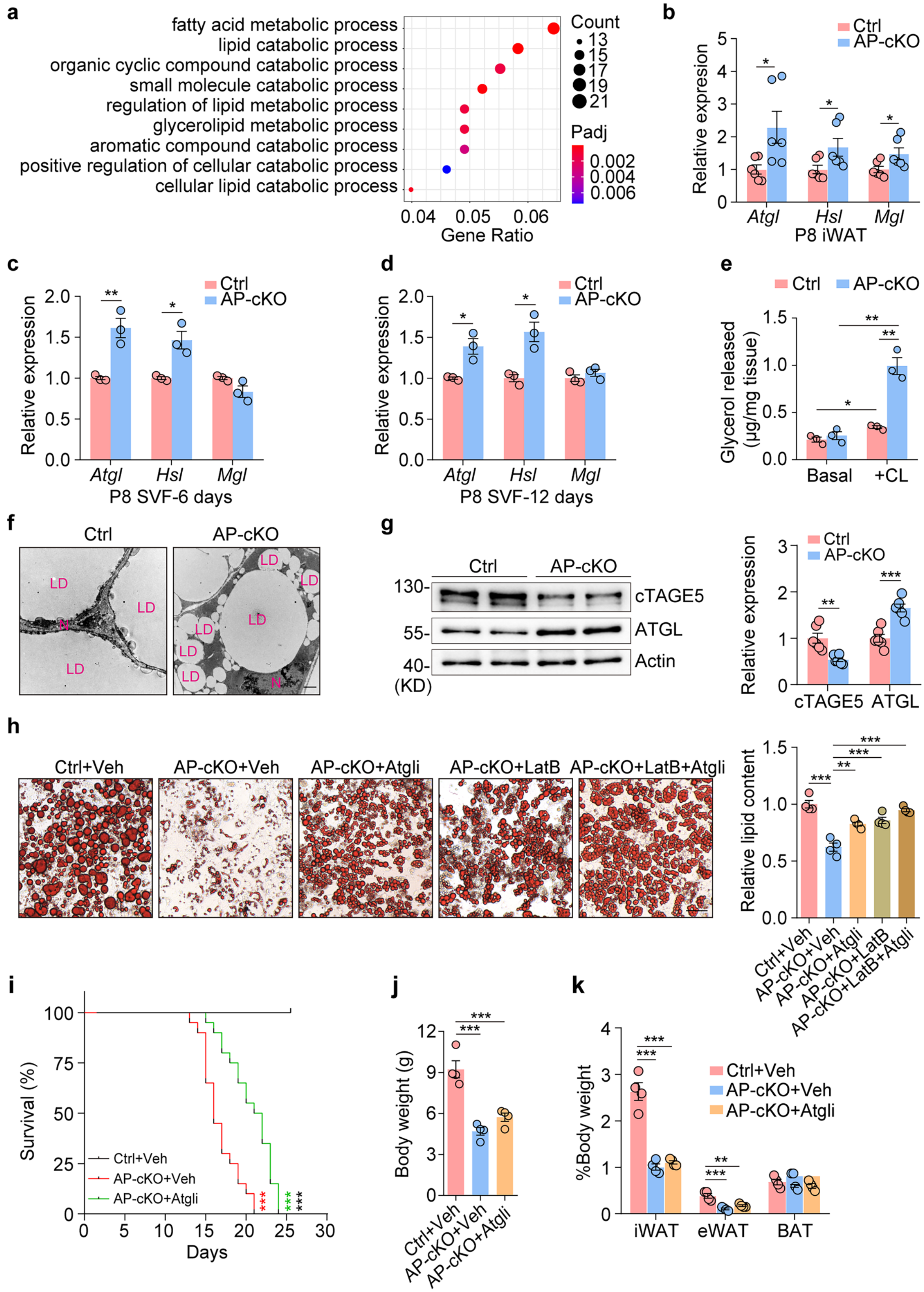

cTAGE5 deficiency in APCs impedes adipocyte differentiation by inhibiting the processing of pro-insulin receptor

To investigate the mechanisms by which cTAGE5 regulates actin cytoskeleton remodeling and lipolysis, we applied gene set enrichment analysis (GSEA) and differential gene expression. We found that genes involved in the phosphatidylinositol 3-kinase /protein kinase B (PI3K/Akt) signaling pathway were significantly downregulated in AP-cKO APCs (Fig. 6a, b), which was verified by the significantly reduced levels of phospho-Akt (p-Akt) (Fig. 6c and Supplementary Fig. 12a). The PI3K/Akt pathway is essential for insulin-mediated function and recognized as an important regulator of adipose tissue development[25,38]. Interestingly, we found that the abundance of pro-insulin receptor (pro-IR)

Fig. 5 | *cTAGE5* deletion in APCs enhances lipolysis in WAT adipocytes. a GO analysis of significantly differentially expressed proteins in iWAT from P8 control and AP-cKO mice. Proteins related to lipid catabolic processes were upregulated in *cTAGE5* AP-cKO iWAT (Ctrl and AP-cKO, *n* = 3 biologically independent mice). Functional enrichment analysis for GO terms was performed using the hypergeometric test, followed by Benjamini–Hochberg correction to control the false discovery rate (FDR). **b** mRNA levels of *Atgl*, *Hsl*, and *Mgl* in P8 iWAT (Ctrl and AP-cKO, *n* = 6 biologically independent samples). **c**, **d** mRNA levels of *Atgl*, *Hsl*, and *Mgl* in SVFs isolated from P8 iWAT after inducing adipocyte differentiation for 6 days (**c**) and 12 days (**d**) (Ctrl and AP-cKO, *n* = 3 biologically independent samples). **e** 10–15 mg iWAT fat pads isolated from P8 mice were stimulated with 250 μl of 2% free fatty acid BSA in the presence or absence of 10 μM CL 316,243 (CL) for 2 hours at 37 °C. Levels of released glycerol in medium were analyzed (Ctrl and AP-cKO, *n* = 3 biologically independent mice). **f** TEM of iWAT from P16 mice (Ctrl and AP-cKO, *n* = 3 biologically independent mice). LD, lipid droplet; N, nucleus. Scale bar, 1 μm. **g** Western blotting and quantitation analysis of cTAGE5 and ATGL in P8 iWAT (Ctrl and AP-cKO, *n* = 6 biologically independent samples). **h** Primary P8 SVFs were treated with Vehicle (Veh, DMSO), 5 μM atglistatin (Atgli) on day 3 after adipogenic cocktail treatment, 1 μM LatB for 2 hours on day 0 and 3 after adipogenic cocktail treatments, or 1 μM LatB concurrently with 5 μM Atgli. Oil Red O staining and quantification of SVFs after inducing adipocyte differentiation for 10 days (Ctrl and AP-cKO, *n* = 4 biologically independent samples). Scale bars, 50 μm. **i** Mice were intraperitoneally injected with Veh (DMSO) or 200 μM/kg Atgli at P8, P11, and P14. Survival of different groups was monitored (Ctrl+Veh, AP-cKO+Veh, and AP-cKO +Atgli, *n* = 20). **j**, **k** Body weight (**j**) and iWAT, eWAT, and BAT (**k**) of mice treated with Veh (DMSO) or Atgli at P16. The ratio to body weight was measured (**k**) (Ctrl and AP-cKO, *n* = 4 biologically independent mice). **b**–**e**, **g**, **j**–**k** Representative of three independent experiments. **h** Representative of four independent experiments. All data are mean ± s.e.m. **P* < 0.05, ***P* < 0.01, and ****P* < 0.001. Unpaired two-tailed Student's *t*-test (**b**–**e**, **g**) or one-way ANOVA followed by Bonferroni post hoc test (**h**, **j**, **k**) or log-rank test (**i**). Source data with exact *P*-value are provided as a Source Data file.

increased significantly in AP-cKO APCs (Fig. 6c and Supplementary Fig. 12a), and the localization of IR on the plasma membrane was reduced by about 47.2% in AP-cKO APCs (Fig. 6d).

IR is synthesized in ER, processed in Golgi, and then transferred from Golgi to the plasma membrane[28,39]. To investigate whether *cTAGE5* deletion impaired the processing of IR, we inspected the distribution of IR through immunostaining with calnexin (ER marker) and ATPase (plasma membrane marker), and observed that IR was mainly co-localized with calnexin and lost most of the co-localization pattern with ATPase in AP-cKO APCs (Fig. 6e). Furthermore, ER, Golgi and plasma membrane were isolated from P8 control and AP-cKO APCs, and the immunoblot results showed that *cTAGE5* deletion led to increased levels of pro-IR/IRβ in the ER and Golgi and decreased levels in plasma membrane (Fig. 6f, g and Supplementary Fig. 12b). Besides, we observed that the morphology of ER was distended and Bip, the ER stress marker, increased significantly in AP-cKO APCs, which might be caused by detention of pro-IR in the ER (Fig. 6c and Supplementary Fig. 12c).

Insulin signaling has been shown to enhance overall lipid storage in adipocyte by promoting triglyceride synthesis and inhibiting lipolysis[40]. We speculated that the enhanced lipolysis in AP-cKO APCs might be due to the impaired insulin signaling caused by disturbed pro-IR processing. To test this hypothesis, primary SVFs isolated from P8 iWAT of control and AP-cKO mice were treated with DMSO or Akt agonist (SC79) during adipogenic cocktail treatment. After 10 days' treatment, SC79 partially enhanced lipid accumulation and total lipid content as determined by Oil Red O staining (Fig. 6h). Additionally, the expression of key lipolytic enzymes (*Atgl*, *Hsl*) in differentiated SVFs decreased significantly under SC79 treatment (Fig. 6i–k). However, SC79 did not improve cytoskeleton remodeling (Supplementary Fig. 12d), which might be possible that insulin-induced cytoskeleton remodeling relied on the IR localization[41]. Moreover, cTAGE5 overexpression in AP-cKO SVFs reduced pro-IR/IRβ levels in the ER and increased their plasma membrane localization (Supplementary Fig. 13a–c). This restoration effectively rescued the impaired adipocyte differentiation by normalizing cytoskeleton remodeling and attenuating the elevated lipolysis during adipocyte differentiation (Supplementary Fig. 13d–i). Collectively, these results demonstrate that cTAGE5 is essential for the processing of pro-IR in the ER, which plays an important role in actin cytoskeleton remodeling and lipolysis during adipocyte differentiation. These processes thereby influence adipogenesis and adipose tissue development (Fig. 7).

Discussion

cTAGE5 has been shown to be important for lipoprotein trafficking and lipid profiles in the liver and brain. In this study, we reveal the essential role of cTAGE5 in the processing of pro-IR in APCs, which is important for adipocyte differentiation and maturation. Ablation of *cTAGE5* specifically in APCs impairs adipose development in neonatal mice, resulting in progressive loss of WAT and death. Knockout of *cTAGE5* in APCs disrupts pro-IR processing, thereby disturbing cytoskeleton remodeling and enhancing lipolysis during adipocyte differentiation (Fig. 7).

Adipogenesis is the process during which APCs undergo coordinated and multifaceted changes in gene expression and protein content as they differentiate into mature adipocytes[17,42,43]. Although adipocyte hypertrophy and hyperplasia during adult obesity have been extensively studied[16,44], the mechanisms that govern APCs differentiation are poorly understood. In this study, we demonstrate that *cTAGE5* deficiency in APCs results in impaired adipocyte differentiation of SVFs and progressive loss of WAT, ultimately leading to mice death at about P21. The phenotype is reminiscent of Berardinelli-Seip congenital lipodystrophy (BSCL) disease in humans. Knocking out the main causative genes *Bscl2* or *Agpat2* also results in severe loss of WAT and premature death in 21% and 80% of mice, respectively[45]. However, *cTAGE5* AP-cKO mice exhibit 100% immature mortality, suggesting that the physiological function of cTAGE5 may be more robust in adipose tissue development and lipid metabolism homeostasis. Additionally, cTAGE5 function is consistent during adipocyte differentiation of hADSC, indicating its conserved role in humans. Previous findings show that PDGFRA$^+$ progenitors contribute to both BAT and WAT formation with distinct regulatory mechanisms[46,47]. Although PDGFRA$^+$ progenitors contribute to BAT formation[48], other report also indicates that PDGFRA expression in BAT progenitor cells has a signaling function to avoid adipose progenitor differentiation[49]. We show here that *cTAGE5* deletion does not affect the BAT mass and mRNA levels of transcription factors associated with BAT function, suggesting that *cTAGE5* loss may have a dispensable effect on BAT formation. Meanwhile, *cTAGE5* deletion by *Adiponectin-Cre* in mature adipocytes has no significant effect on white adipose tissue and metabolic dysfunction, implying that cTAGE5 plays a critical role primarily during the neonatal developmental period.

Previous reports have shown that cytoskeleton remodeling is essential for adipocyte differentiation and the formation of mature adipocytes[20,21]. We show that *cTAGE5* deletion in APCs leads to the significant down-regulation of a group of actin cytoskeleton-related genes, represented by *Myl9*. MYL9 is expressed at high levels in WAT-derived APCs[50,51], and binds to actin filaments to control cytoskeleton dynamics[35,52]. We demonstrate that MYL9 is critical for adipocyte differentiation of 3T3-L1 preadipocytes. Importantly, the inhibitors of actin polymerization, but not inhibitors of tubulin polymerization, can effectively rescue the defect in adipocyte differentiation of *cTAGE5* AP-cKO APCs. The collective findings indicate a compelling possibility that actin cytoskeleton remodeling could regulate cell fate decisions. However, it is unclear how the ER-localized cTAGE5 regulates APCs'

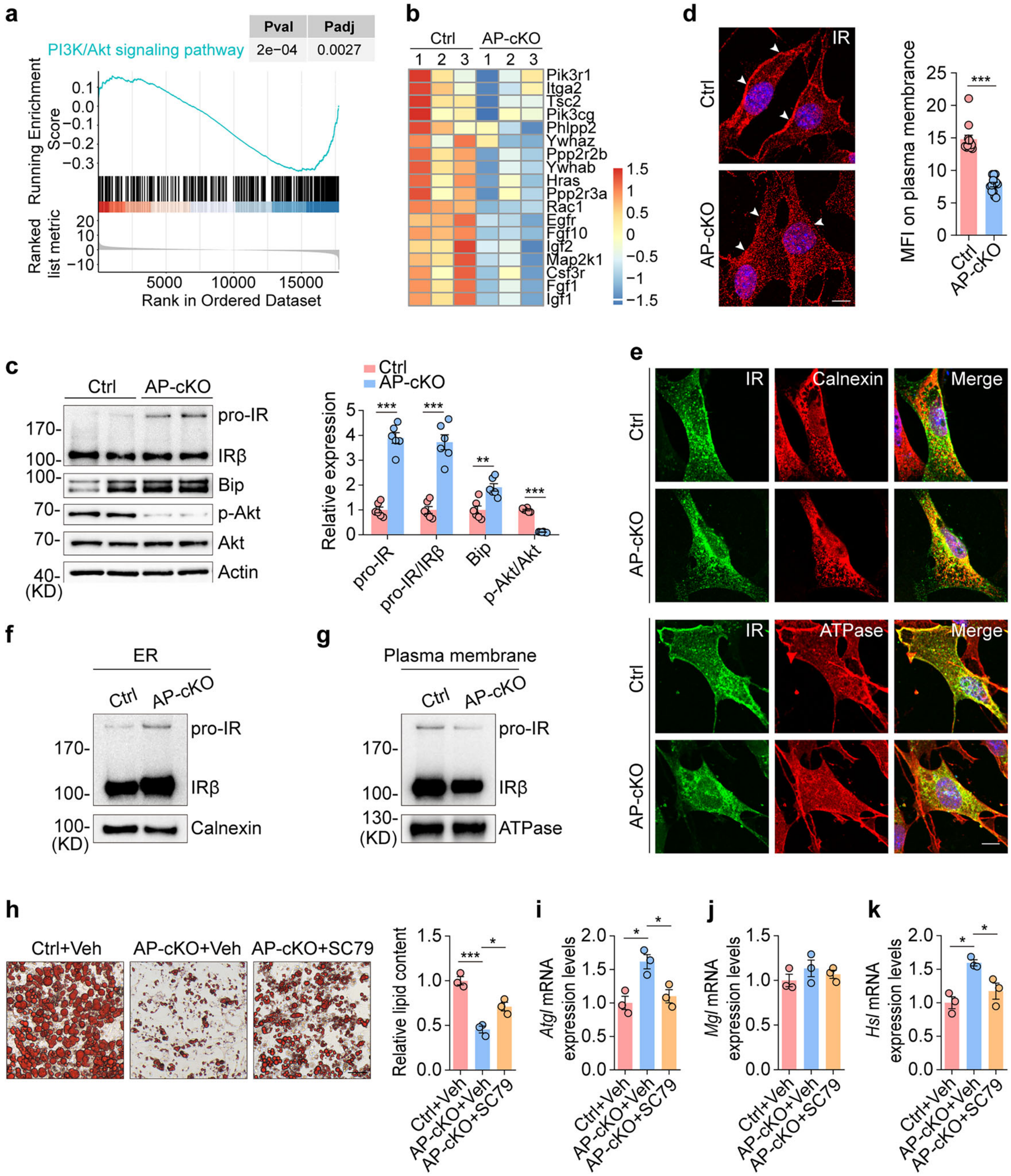

Fig. 6 | *cTAGE5* deletion in APCs disturbs the processing of pro-IR. a Running enrichment score of GSEA comparison of the genes in APCs from P8 control and AP-cKO mice. Statistical significance (adjusted *P*-value < 0.05) was determined by the phenotypic-based permutation test for GSEA. The Benjamini–Hochberg method was used to calculate adjusted *P*-values for multiple hypothesis testing. **b** Heatmap of leading genes' expression from GSEA. PI3K/Akt signaling pathway-related genes are downregulated in P8 AP-cKO APCs. **c** Western blotting analysis of pro-IR/IRβ, Bip, p-Akt/Akt in P8 SVFs and quantification by normalization to actin (Ctrl and AP-cKO, $n = 6$ biologically independent samples). **d** Immunofluorescence staining of IR in P8 SVFs and the mean fluorescence intensity (MFI) on the plasma membrane was quantified (Ctrl and AP-cKO, $n = 3$ biologically independent samples). Scale bar, 10 μm. **e** Double immunofluorescence staining of IR (green) and calnexin (ER marker, red) or ATPase (plasma membrane marker, red) in P8 SVFs (Ctrl and AP-cKO, $n = 3$ biologically independent samples). Scale bar, 10 μm. **f**, **g** Protein levels of pro-IR/IRβ in the separated ER (**f**) and plasma membrane (**g**) fractions from P8 SVFs. **h**–**k** Primary P8 SVFs were treated with Vehicle (Veh, DMSO) or 10 μM Akt agonist (SC79) during adipogenic cocktail treatment. Oil Red O staining and quantification of SVFs after inducing adipocyte differentiation for 10 days (**h**) (Ctrl and AP-cKO, $n = 3$ biologically independent samples). Scale bars, 50 μm. mRNA levels of *Atgl* (**i**), *Mgl* (**j**), and *Hsl* (**k**) in SVFs after inducing adipocyte differentiation for 10 days (Ctrl and AP-cKO, $n = 3$ biologically independent samples). **c**–**k** Representative of three independent experiments. All data are mean ± s.e.m. $^{*}P < 0.05$, $^{**}P < 0.01$, and $^{***}P < 0.001$. Unpaired two-tailed Student's *t*-test (**c**, **d**) or one-way ANOVA followed by Bonferroni post hoc test (**h**–**k**). Source data with exact *P*-value are provided as a Source Data file.

cytoskeleton remodeling, although previous reports have shown that cTAGE5 participates in vesicle trafficking, which is transported along the cytoskeleton. Whether *cTAGE5* deficiency affects the cytoskeleton by causing disturbances in vesicle trafficking or affects cytoskeleton remodeling through targeting actin directly or indirectly remains to be answered. Besides, cell cycle arrest has been suggested to be necessary for adipocyte differentiation[13]. *cTAGE5* deletion leads to an increase of APCs in G1 phase, but a decrease in G0 phase in P8 SVFs. The increased

https://doi.org/10.1038/s41467-025-60698-1

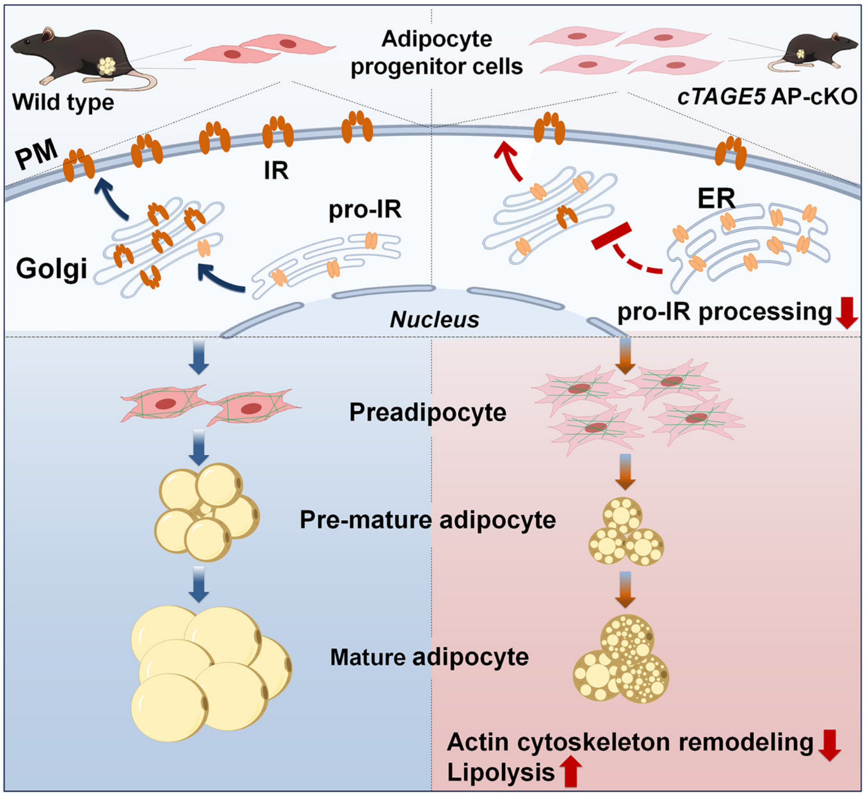

Fig. 7 | Scheme for the roles of cTAGE5 in adipogenesis. *cTAGE5* deletion in APCs disturbs the processing of pro-IR, thereby disrupting actin cytoskeleton remodeling and enhancing lipolysis during adipocyte differentiation, ultimately compromising the process of adipogenesis and adipose tissue development. Wild type: *cTAGE5*$^{flox/+}$ or *cTAGE5*$^{flox/flox}$; *cTAGE5* AP-cKO: *cTAGE5*$^{flox/flox}$*;Pdgfrα-Cre*; pro-IR: pro-insulin receptor; IR: insulin receptor; PM: plasma membrane; ER: endoplasmic reticulum; Golgi: golgi apparatus. [Figure created with Biorender.com].

G1 phase is the cause or result of adipocyte differentiation impairment remains to be determined.

Of note, *cTAGE5* deficiency in APCs results in increased serum glycerol and NEFA levels in P8, but not in P16 AP-cKO mice. This may be because the severe loss of WAT in P16 AP-cKO mice leads to a smaller amount of glycerol when lipolysis is stimulated. To test this possibility, we perform ex vivo lipolysis experiments and find a significantly higher level of released glycerol under stimulated conditions in P16 AP-cKO iWAT than in controls when normalized to the weight of fat pads. In addition, TEM result shows that *cTAGE5* deficiency in APCs results in the presence of many smaller lipid droplets in P16 adipocytes. This confirms the acceleration of lipolysis and can explain the progressive reduction in WAT in AP-cKO mice starting at P8.

Several studies have shown that lipolysis plays an essential role in the white adipocyte maturation, particularly during the differentiation of preadipocytes into mature adipocytes[22,53]. In this study, we find that the levels of proteins related to lipid catabolic process, including the rate-limiting enzyme ATGL, are significantly upregulated in *cTAGE5* AP-cKO iWAT. As a critical regulator of lipolysis, ATGL is indispensable for maintaining the dynamic balance between lipid storage and mobilization[37,54,55]. Previous research indicates that ATGL expression increases during 3T3-L1 adipocyte differentiation, peaking at the stage of visible lipid droplets[56]. Although lipid droplet formation and remodeling during differentiation require active lipolysis, mature adipocytes exhibit more stable lipid droplets and less lipolysis activity to prioritize lipid storage and energy balance[57]. Furthermore, accumulating evidences reveal that adiponectin secreted by mature adipocytes not only enhances insulin-mediated suppression of lipolysis but also independently inhibits the process[58]. This could explain why *cTAGE5* deletion in mature adipocytes does not result in an aberrant phenotype, which might be due to a stabilized cytoskeleton and lower lipolysis activity compared to APCs. These hypotheses, however, warrant further investigation. Meanwhile, recent studies have reported that the translocation of ATGL between lipid droplets and the ER is involved in the regulation of lipolysis[54]. Importantly, the ATGL inhibitor effectively restores adipocyte differentiation impairment in vitro, however, its impact is limited in AP-cKO mice. This underscores the need for further investigation of the contribution in vivo microenvironment to adipocyte differentiation.

Insulin signaling enhances overall lipid storage in adipocytes by promoting triglyceride synthesis and inhibiting lipolysis and is recognized as an important regulator of adipogenesis. The levels of pro-IR increased significantly, and the levels of p-Akt decreased significantly in AP-cKO SVFs. Meanwhile, *cTAGE5* deletion leads to IR retention in the ER and reduced distribution on the plasma membrane, accompanied by ER morphological distention and ER stress. Since cTAGE5 plays an important role in vesicle trafficking, it can be speculated that the enhanced lipolysis would be due to the impaired insulin signaling caused by the disturbed processing of pro-IR. Intriguingly, Akt agonist (SC79) can partially rescue adipocyte differentiation and downregulate the expression of lipolytic enzymes in AP-cKO SVFs. However, the cytoskeleton remodeling cannot be improved, implying that insulin-induced cytoskeleton remodeling relies on the IR localization.

In summary, we reveal the essential role of cTAGE5 in the differentiation of APCs and adipose tissue homeostasis during the neonatal period and elucidate the potential mechanisms. Given the importance of WAT expansion in body growth, metabolic homeostasis, and endocrine regulation in the neonatal period, our findings would not only improve the understanding of the pathological mechanisms of defective adipogenesis but also provide insight into the development of new therapeutic approaches to treat relevant metabolic disorders.

Methods

Mice

cTAGE5$^{flox/flox}$ mice were generated previously[33]. *cTAGE5* was specifically deleted in APCs by mating *cTAGE5*$^{flox/flox}$ mice with *Pdgfrα-Cre* mice (The Jackson Laboratory, 013148). To delete *cTAGE5* in mature adipocytes, *cTAGE5*$^{flox/flox}$ mice were crossed with *Adiponectin-Cre* mice, which were obtained from Wanzhu Jin lab (Institute of Zoology, Chinese Academy of Sciences). All mice were of the C57BL/6 J background and were housed at 23 °C ± 2 °C with a humidity of 50%–65% under a 12 hours light/dark cycle with free access to food and water. Tail biopsies were used to extract genomic DNA for genotyping. During the experimental procedures, the mice were anesthetized with 3% isoflurane, and all animal protocols were performed according to the ethical principles of animal welfare of the Beijing Institute of Neurosurgery.

Isolation of primary SVFs

iWAT isolated from mice was rinsed three times in phosphate-buffered saline (PBS, Biosharp, BL302A) with 10% fetal bovine serum (FBS, Hyclone, SH30406.05) and 1% penicillin–streptomycin (PS, Gibco,15140122), weighed, minced into 1–2 mm^3 pieces, and digested in 1 mg/ml type I collagenase (Sigma-Aldrich, C2674) containing 20% FBS in PBS for 30 minutes at 37 °C with a vigorous shaking every 10 minutes. After digestion, an equal volume of cultured medium was added and centrifuged at 300 × *g* for 5 minutes. The floating adipocytes were discarded, and the pelleted SVFs were resuspended in PBS containing 2% FBS, washed two times, filtered through sterile 70 μm mesh filters (Falcon, 352350), and then cultured in DMEM/F12 (Gibco,11330032) supplemented with 10% FBS, 1% GlutaMAX (Gibco, 35050061), and 1% PS[59]. Twenty-four hours later, the medium was aspirated, and fresh medium was added. The primary SVFs were cultured for 5–7 days until confluence.

Flow cytometry and cell sorting

For phenotypical APCs analysis and sorting, the primary SVFs were stained with the following surface antibodies for 30 minutes at 4 °C: CD45 PE (Invitrogen, 12-0451-83, 1:160 dilution); Ter119 PE (BioLegend, 116207, 1:80 dilution); CD31 PE (BD Biosciences, 553373, 1:100 dilution); CD34 eFluor450 (Invitrogen, 48-0341-82, 1:40 dilution); SCA-1 APC-Cy7 (BioLegend, 108146, 1:80 dilution); CD29 PE-Cy7 (Invitrogen, 25-0291-82, 1:40 dilution); PDGFRA APC (Invitrogen, 17-1041-81, 1:20 dilution). After antibody incubation, the primary SVFs were washed in PBS containing 2% FBS, centrifuged at 300 × *g* for 5 minutes, and analyzed or sorted with a BD FACSAria III. For Ki67 staining, after incubation with surface antibodies, the primary SVFs were fixed with fixation/permeabilization solution for 40 minutes at 4 °C, washed two times with permeabilization buffer, and then stained with Ki67 PerCP-Cyanine5.5 (Invitrogen, 46-5698-82, 1:250 dilution) for 30 minutes at 4 °C. The samples were washed and analyzed with the BD FACSAria III. For EdU staining, P8 control and AP-cKO mice were injected with 100 mg/kg EdU intraperitoneally for 3 days. Then, primary SVFs were isolated and stained with the following surface antibodies for 30 minutes at 4 °C: CD45 PerCP-Cyanine5.5 (Invitrogen, 45-0451-82, 1:160 dilution); CD34 eFluor450 (Invitrogen, 48-0341-82, 1:40 dilution); CD29 APC (Invitrogen, 17-0291-80, 1:80 dilution); and SCA-1 AF700 (Invitrogen, 56-5981-82, 1:40 dilution). After antibody incubation, the detection of EdU was performed according to the protocol of the manufacturer (Invitrogen, C10425). For Annexin V staining, after incubation with surface antibodies, the primary SVFs were resuspended in 1× binding buffer and then stained with Annexin V FITC (BD Biosciences, 556547) for 15 minutes at room temperature. Then, the samples were washed, added 7-AAD for 10 minutes at room temperature, and analyzed with the BD FACSAria III within 1 hour. All data were analyzed by FlowJo software (version 10.8.1).

Cell culture and induction of differentiation

All cells were grown at 37 °C in a 5% CO_2 humid atmosphere. 3T3-L1 preadipocytes (Cell Resource Center, Peking Union Medical College; NSTI-BMCR) were cultured in DMEM (Hyclone, 11995065) supplemented with 10% NBCS (Every Green, 22011-8612). hADSC cells (Procell, CP-H202) were cultured in mesenchymal stem cell medium (ScienCell, 7501). For primary SVFs, 3T3-L1 cells, and hADSC cells, 2 days after confluence (0 day), they were induced in DMEM/F12 (SVFs) or DMEM (3T3-L1/hADSC) consisting of 10% FBS, 1 μM dexamethasone (Sigma-Aldrich, D4902), 0.5 mM 3-isobutyl-1-methylxanthine (IBMX, Sigma-Aldrich, I7018), 10 μg/ml insulin (Macgene, CC101), and 2.5 μM rosiglitazone (Macgene, CH004) for 3 days. The culture medium was replaced with DMEM/F12 (SVFs) or DMEM (3T3-L1/hADSC), consisting of 10% FBS and 10 μg/ml insulin, for another 2 days. Then, the culture medium was replaced with DMEM/F12 (SVFs) or DMEM (3T3-L1/hADSC) containing 10% FBS every other day until 10–12 days. The formation of lipid droplets was observed by Oil Red O (Solarbio, O8010) staining[60]. The differentiated adipocytes were fixed in 4% paraformaldehyde (Solarbio, P1110) for 10 minutes at room temperature and then incubated in Oil Red O working solution consisting of 4 ml of Oil Red O stock solution (0.3% in isopropanol) and 2 ml of ddH_2O for 20 minutes protected from light. After incubation, the cells were washed gently three times with ddH_2O and photographed. The TG contents were extracted with 100% isopropanol and detected by measuring the optical density at 570 nm through a microplate reader (Spark, TECAN).

Glucose and insulin tolerance tests

Glucose tolerance tests were conducted after 16 hours of starvation with free access to water, and then mice were intraperitoneally injected with 2 mg/g body weight of D-glucose (Sigma-Aldrich, G8270). Insulin tolerance tests were conducted after 6 hours of starvation with free access to water,r and then intraperitoneally injected with 0.75 units/kg of body weight human insulin (Novolin). Blood glucose levels were measured at the indicated times by Roche ACCU-CHEK Performa.

Western blotting

The tissues or cells were lysed with RIPA lysis buffer containing 50 mM Tris-HCl, pH 7.4, 1 mM EDTA, 150 mM NaCl, 1% NP40, 0.5% sodium deoxycholate, and protease inhibitors for 15 minutes on ice. After sonication (100 W, 5 seconds pulses with 5 seconds intervals, 3 cycles), cell lysates were centrifuged at 12,000 × *g* for 10 minutes at 4 °C, and the supernatant was collected. Protein concentration was determined using the Bradford assay (Bio-Rad, 500205) with bovine serum albumin (BSA, NEB, O0817) as a standard. Briefly, 10 μl of each protein sample was mixed with 1 ml of Bradford reagent and incubated at room temperature for 5 minutes. Absorbance was measured at 595 nm using a microplate reader (Spark, TECAN). A standard curve was generated with known concentrations of BSA (0–1 μg/μl), and sample protein concentrations were calculated based on the standard curve. Subsequently, 5× SDS loading buffer was added to the supernatant and denatured at 95 °C for 5 minutes for western blotting. The following antibodies were used for western blotting: cTAGE5 (Sigma-Aldrich, HPA000387, 1:2000 dilution); actin (TransGen, HC201, 1:2000 dilution); α-tubulin (Cell Signaling Technology, 3873s, 1:3000 dilution); GAPDH (Cell Signaling Technology, 2118s, 1:2000 dilution); MYL9 (Abcam, ab191393, 1:1000 dilution); ATGL (Proteintech, 55190-1-AP, 1:1000 dilution); IRβ (Cell Signaling Technology, 23413, 1:1000 dilution); Bip (Abcam, ab21685, 1:10000 dilution); p-Akt (Cell Signaling Technology, 4060, 1:1000 dilution); Akt (Cell Signaling Technology, 4691, 1:1000 dilution); calnexin (Thermo Fisher, MA3-027, 1:1000 dilution); ATPase (Abcam, ab76020, 1:2000 dilution); Flag (MBL, M185, 1:3000 dilution); and Myc (MBL, M562, 1:2000 dilution). Horseradish peroxidase (HRP)-conjugated secondary antibodies included anti-rabbit IgG (CWBIO, CW0103, 1:5000 dilution) and anti-mouse IgG

(CWBIO, CW0102, 1:5000 dilution). Immunodetection was performed using chemiluminescent HRP substrate (Millipore, WBKLS0500) and detected with a chemiluminescent imaging system (SageCreation).

Hematoxylin and eosin (H&E) staining and immunostaining

Tissues were fixed with 4% paraformaldehyde, dehydrated in a graded ethanol series, embedded in paraffin, and sectioned at a thickness of 5 μm by a Leica RM2255 rotary microtome. For H&E staining, the sections were deparaffinized, rehydrated, stained with hematoxylin for 10 minutes and eosin for 40 seconds, dehydrated, and mounted. Sections were photographed with the EVOS FL Auto 2 Imaging System (Thermo Fisher Scientific) and analyzed with ImageJ software. The cell area distribution of adipocytes was calculated using Adiposoft software (1.16). For FITC-phalloidin staining, primary SVFs cultured on coverslips were fixed with 4% paraformaldehyde for 15 minutes at room temperature, permeabilized with PBS containing 0.3% Triton X-100 (ZSGB-BIO, ZLI-9308) and 3% bovine serum albumin (BSA, Sigma-Aldrich, B2064) for 10 minutes, stained with FITC-phalloidin (Solarbio, CA1620, 1:200 dilution) and 4,6-diamidino-2-phenylindole (DAPI, Solarbio, C0060, 1:1000 dilution) in PBS containing 1% BSA for 30 minutes at room temperature, and mounted. For immunostaining, primary SVFs cultured on coverslips were fixed with 4% paraformaldehyde for 20 minutes at room temperature, blocked with 5% BSA for 1 hour, and incubated with primary antibody overnight at 4 °C. The following antibodies were used for immunostaining: cTAGE5 (Sigma, HPA000387, 1:250 dilution); PDGFRA (Abcam, ab203491, 1:300 dilution); α-tubulin (Cell Signaling Technology, 3873 s, 1:400 dilution); IRβ (Cell Signaling Technology, 23413, 1:100 dilution); calnexin (Thermo Fisher, MA3-027, 1:200 dilution); ATPase (Abcam, ab76020, 1:300 dilution). After incubation, the coverslips were washed with PBS and incubated with secondary antibody (Invitrogen) and DAPI for 1 hour at room temperature. The fluorescent photographs were taken with a Zeiss LSM 700 (Carl Zeiss, Germany) confocal microscope equipped with a 100× oil immersion objective (1.4 numerical aperture (NA)) and analyzed with ImageJ software (Fiji, version 1.53c).

Lentivirus shRNA knockdown of cTAGE5 and MYL9

The following shRNAs were purchased from YILE Biotech (Shanghai, China): mouse *cTAGE5* (target sequence CCGGCAAGTGAATGATCTCGATAAACTCGAGTTTATCGAGATCATTCACTTGTTTTTG); mouse *Myl9* (target sequence CCGG GATAAGAAGGGCAACTTCAACCTCGAGGTTGAAGTTGCCCTTCTTATCTTTTTG); and the negative control (target sequence CCGGCAACAAGATGAAGAGCACCAACTCGAGTTGGTGCTCTTCATCTTGTTGTTTTTG). The following shRNAs were purchased from OBiO technology (Shanghai, China): human *cTAGE5* (target sequence CCGGATGAATTGATGGCGGATATTTCTCGAGAAATATCCGCCATCAATTCATTTTTTTG); and negative control (target sequence CCGGCCTAAGGTTAAGTCGCCCTCGCTCGAGCGAGGGCGACTTAACCTTAGGTTTTTTG). The lentiviruses expressing shRNA were packaged with a four-plasmid system following the manufacturer's instructions. For the construction of cTAGE5 knockdown or MYL9 knockdown cell lines, the cells (3T3-L1/hADSC) were cultured in a 24-well plate and infected with lentivirus. Then, the cells were transferred to a 6-cm dish at 80%–90% confluence and treated with 3 μg/ml (3T3-L1) or 2 μg/ml (hADSC) puromycin (Gibco, A1113803) for several passages until almost all cells were infected with lentivirus. After that, the stable cell line was maintained with half the concentration of puromycin.

Genotyping polymerase chain reaction (PCR) and real-time PCR

Genomic DNA was extracted from mouse tail biopsies using an alkaline lysis protocol. Briefly, tissue samples were digested in 100 μl solution A consisting of 25 mM NaOH and 0.2 mM EDTA, then the tubes were heated at 95 °C for 1 hour. Later, 100 μl solution B, consisting of 40 mM Tris-HCl, pH 8.0, was added to neutralize solution A. The DNA extract was used directly as a template for genotyping PCR with the following primer pairs. For *flox* fragment: forward: 5′-GACACTTGACCCCTCCTCTCC-3′ and reverse: 5′-AACGGCTCATGCTTGCTAACC-3′; for *Pdgfrα-Cre*: forward: 5′-GCGGTCTGGCAGTAAAAACTATC-3′ and reverse: 5′-GTGAAACAGCATTGCTGTCACTT-3′; for *Adiponectin-Cre*: 5′-CGGCATGGTGCAAGTTGAAT-3′ and reverse: 5′- TCAGCTACACCAGAGACGGA-3′. Total RNA was extracted from tissues or cells using TRIzol reagent (Invitrogen, 15596018CN). The concentration and purity of RNA were detected by a spectrophotometer (Thermo Fisher Scientific, Nano3000). Then, 1 μg of total RNA was reverse transcribed using a PrimeScript RT Reagent Kit (TaKaRa, RR047A). Real-time PCR was performed according to the manufacturer's protocol. The mRNA expression level was normalized to actin and analyzed according to the $2^{-\Delta\Delta Ct}$ method. The primers for real-time PCR are listed in Supplementary Data 1.

Transmission electron microscopy (TEM)

iWAT isolated from mice was immediately fixed in 2.5% glutaraldehyde (Electron Microscopy Sciences, 16220) in 0.1 M phosphate buffer (pH 7.4) for 2 hours at 4 °C. Post-fixation was in 1% osmium tetroxide (Sigma-Aldrich, 1.24505) for 1.5 hours at room temperature. Samples were then dehydrated through a graded acetone series (Sigma-Aldrich, 270725) and infiltrated with EPON812 resin (2:1 acetone: resin for 1 hour, 1:2 acetone: resin for 1 hour, pure resin overnight at 4 °C). The resin-embedded samples were polymerized at 70 °C for 16 hours in a drying oven, then gradually cooled and maintained in a vacuum desiccator[33]. Ultra-thin sections were cut on a Leica ultramicrotome with a diamond knife, mounted on 200-mesh copper grids, and stained with uranyl acetate (2% in 50% methanol) for 10 minutes followed by lead citrate for 5 minutes. Images were acquired using a Hitachi H-7650 transmission electron microscope operated at 80 kV.

Ex vivo lipolysis assay and serum lipid analysis

For ex vivo lipolysis, iWAT isolated from mice was cut into 10–15 mg fat explants and rinsed two times in cold PBS. The fat explants were distributed into 48-well plates (Corning), minced into 1–2 mm^3 pieces, and incubated with 250 μl of phenol red free DMEM (Gibco, A1443001) supplemented with 2% free fatty acid BSA (Solarbio, A8850) in the presence or absence of 10 μM CL 316,243 (Cayman Chemical, 17499) for 2 hours at 37 °C. The supernatant was collected, and released glycerol levels were detected by a cell-based glycerol assay kit (Abcam, ab133130). Serum TG (Applygen, E1003), TC (Applygen, E1005), and glycerol (Sigma-Aldrich, MAK117) were measured colorimetrically according to the manufacturers' instructions.

Cellular fractionation

Endoplasmic reticulum was separated from P8 SVFs using an endoplasmic reticulum protein isolation kit (Solarbio, EX1931). Golgi apparatus was separated from P8 SVFs using a golgi apparatus protein isolation kit (Solarbio, EX1240). The plasma membrane was separated from P8 SVFs using a plasma membrane protein isolation kit (Minute, SM-005). The procedures were performed according to the manufacturer's instructions.

Library preparation for RNA sequencing (RNA-seq)

Primary SVFs were isolated from P8 control and AP-cKO mice, and the $Lin^{-}CD29^{+}CD34^{+}SCA\text{-}1^{+}$ cell population was isolated. Then, total RNA was extracted from this cell population. The RNA quality was ascertained by determining purity with a NanoPhotometer® spectrophotometer (IMPLEN), measuring concentration using the Qubit® RNA Assay Kit in a Qubit® 2.0 fluorometer (Life Technologies), and assessing integrity with the RNA 6000 Nano assay kit (Agilent Technologies). The library preparation process began with the use of at least 5 ng of RNA per sample, following the SMARTer Ultra-low input RNA protocol by Berry Genomics (Beijing, China). In brief, the mRNA was purified using poly (T) oligo-attached magnetic beads, fragmented with divalent cations in NEBNext first-strand synthesis reaction buffer, and the cDNA was synthesized. The libraries were constructed by converting overhangs into blunt ends, ligating NEBNext adapters, and selecting fragments in the range of 150 base pairs (bp) using an AMPure XP system, with the library quality assessed on an Agilent Bioanalyzer 2100 system. Then, clustering and sequencing were performed by clustering the index-coded samples on a cBot cluster generation system with a TruSeq PE cluster kit v3-cBot-HS (Illumina) and then sequencing on the Illumina NovaSeq 6000 platform to generate 150-bp paired-end reads. During data cleaning and analysis, specific types of reads were first removed from the dataset. These included reads containing adapters, those with more than three 'N' bases, and reads where over 20% of the nucleotides had a Phred score ≤5. After this filtration, key quality indicators, such as Q20, Q30, and the GC content of the remaining 'clean' data, were calculated.

Library alignment and Differential gene expression (DEG) analysis

The clean reads were mapped to the Silva database to remove rRNA and aligned to Ensembl mouse GRCm38 (mm10) genomes using Hisat2 software (version 2.2.1). FeatureCount (version 2.0.2) was used for the quantification of reads mapped to each gene. DESeq2 (version 1.26.0) was employed to conduct differential expression analysis of the genes (Supplementary Data 2)[61], where a two-tailed Wald test was used for statistical significance. To control the false discovery rate, the *P*-value obtained from this analysis was adjusted using the Benjamini–Hochberg method. Genes that exhibited an absolute fold change greater than 1.5 and had an adjusted $P < 0.05$ were classified as differentially expressed.

Mass spectrometry analysis

Three biological replicates of iWAT samples were isolated from P8 control and AP-cKO mice and lysed with RIPA lysis buffer. For quantitative proteomic analysis, three biological replicates of cell lysates (30 μg of protein per sample) were run on SDS-PAGE gel and stained with Coomassie brilliant blue reagent. All bands were excised from the electrophoresis gel and digested with trypsin (Sigma-Aldrich, T6567) at 37 °C overnight. The tryptic peptides were analyzed on an Easy-nLC 1200 HPLC system (Thermo Fisher Scientific) coupled to an Orbitrap Exploris 480 (Thermo Fisher Scientific). All samples were reconstituted in 0.1% formic acid (FA) and separated on a fused silica trap column (100 μm ID * 2 cm) in-house packed with reversed-phase silica (Sunchrom C18, 5 μm, USA) coupled to an analytical column (75 μm ID * 20 cm) packed with reversed-phase silica (Sunchrom C18, 3 μm, USA). The peptides were analyzed with 90 minutes gradient (buffer A: 0.1% FA in H2O, buffer B: 80% acetonitrile (ACN), 0.1% FA in H2O) at a flow rate of 300 nl/minutes (8–12% B, 8 minutes; 12–30% B, 50 minutes; 30–40% B, 12 minutes; 40–95% B, 1 minutes; 95% B, 14 minutes). MS data were acquired using an Orbitrap mass analyzer in data-dependent acquisition mode. The cycle time was set as 2 seconds. The spray voltage of the nano-electrospray ion source was 2.3 kV, and the heated capillary temperature was 350 °C. Full scan MS data were collected at a high resolution of 120,000 (m/z 200) from 350 to 1500 m/z. The automatic gain control target was 300%, dynamic exclusion was 30 seconds, and the intensity threshold was $5.0 * 10^4$. The precursor ions were selected from each MS full scan with an isolation width of 1.6 m/z for fragmentation with a normalized collision energy of 28%. For peptide analysis, MS/MS data were acquired at a resolution of 15,000 (m/z 200). The automatic gain control target was 75%; the maximum injection time was 22 milliseconds. The resulting MS/MS data were processed and quantified using Proteome Discoverer software (Thermo Fisher Scientific, version 2.4.1.15) using the SequestHT search engine, and tandem mass spectra were matched against the UniProt *Mus musculus* database (updated November 2022) with common contaminants to identify the peptides. Database searching parameters were set as follows: enzyme specificity for trypsin and up to two missed cleavages were allowed, minimum peptide length was 6, and mass tolerance for precursor and fragment ions was set as 10 ppm and 0.02 Da, respectively. Cysteine carbamidomethylation was set as a fixed modification. For peptide identification, methionine oxidation and acetylation at the N-terminal of proteins were set as variable modifications. The false discovery rate (FDR) was calculated using the Percolator algorithm provided by PD. FDR on peptide and protein levels was 1%. The contaminating proteins were excluded from further data analysis. Precursor ions Quantifier was used for peptides and protein quantification. Protein ratio calculation was based on protein abundances by the statistical tests of the *t*-test (Background Based). Unique peptides that were exclusively expressed in cells or displayed an abundance at least two-fold higher than control, with a statistical significance of $P < 0.05$, were selected. From all these peptides, only those peptides consistently detected in all three replicates were considered as definitive cell-associated proteins.

Gene ontology (GO) enrichment analysis

For enrichment analysis of the differentially expressed genes or proteins, we used the clusterProfiler package (version 3.14.3). This included the application of the 'enrichGO' function for GO enrichment based on the hypergeometric distribution. Adjusted *P*-values (Padj) were shown in the GO dot plot using a continuous color scale, and the size of each dot represented the number of associated proteins. Additionally, GSEA was performed using the 'GSEA' function to further elucidate the biological significance of our findings. The Benjamini–Hochberg method was used for multiple comparison adjustment. Enriched terms with adjusted $P < 0.05$ were retained.

Phenome-wide association study (PheWAS)

To explore the association of *cTAGE5/MIA2* with lipid metabolism phenotypes, we conducted PheWAS based on data from the UK Biobank[62,63] and concluded genome-wide association study (GWAS) summary data of eight lipid metabolism related phenotypes in the PheWAS, including apolipoprotein B (ApoB), body mass index (BMI), cholesterol (Chol), glucose (Glu), hemoglobin A1c (Hb1Ac), high-density lipoprotein (HDL), LDL, and TG. We set $P < 1 \times 10^{-5}$ as the threshold to indicate significance.

Genotyping data of *cTAGE5/MIA2* and LDL measurement were obtained from previous research[64]. The association test was performed by the GCTA software (version 1.94.1) suite with a mixed linear model. Three batches of association results were further combined by the meta-analysis module of the PLINK software (version 1.9) suite.

Statistical analysis

All data were acquired from three or four independent experiments and were presented as mean ± s.e.m. An unpaired two-tailed Student's *t*-test was used for two-sample comparisons. One-way ANOVA was performed for multiple comparisons with one variable, followed by the Bonferroni post hoc test. Two-way ANOVA was applied for multiple comparisons with two independent variables, followed by a Bonferroni post hoc test. All data were visualized using GraphPad Prism software (version 8.0), and $P < 0.05$ was considered statistically significant.

Reporting summary

Further information on research design is available in the Nature Portfolio Reporting Summary linked to this article.

Data availability

The raw sequencing data used to generate Figs. 4a–c and 6a, b have been deposited in the GSA database (Genome Sequence Archive in

National Genomics Data Center, China National Center for Bioinformation/Beijing Institute of Genomics, Chinese Academy of Sciences) with the accession number CRA021972 [https://ngdc.cncb.ac.cn/gsa/]). The mass spectrometry proteomics data for Fig. 5a and Supplementary Fig. 11e have been deposited to the ProteomeXchange Consortium (http://proteomecentral.proteomexchange.org) via the iProX partner repository with the dataset identifier PXD059525. All other data are provided in the Supplementary Information/Source Data file. Source data are provided with this paper.

References

1. Zwick, R. K., Guerrero-Juarez, C. F., Horsley, V. & Plikus, M. V. Anatomical, physiological, and functional diversity of adipose tissue. *Cell Metab.* **27**, 68–83 (2018).
2. Chouchani, E. T. & Kajimura, S. Metabolic adaptation and maladaptation in adipose tissue. *Nat. Metab.* **1**, 189–200 (2019).
3. Walther, T. C., Chung, J. & Farese, R. V. Lipid droplet biogenesis. *Annu. Rev. Cell Dev. Biol.* **33**, 491–510 (2017).
4. Ghaben, A. L. & Scherer, P. E. Adipogenesis and metabolic health. *Nat. Rev. Mol. Cell Biol.* **20**, 242–258 (2019).
5. Holtrup, B. et al. Puberty is an important developmental period for the establishment of adipose tissue mass and metabolic homeostasis. *Adipocyte* **6**, 224–233 (2017).
6. Han, J. et al. The spatiotemporal development of adipose tissue. *Development* **138**, 5027–5037 (2011).
7. Wang, Q. A., Tao, C., Gupta, R. K. & Scherer, P. E. Tracking adipogenesis during white adipose tissue development, expansion and regeneration. *Nat. Med.* **19**, 1338–1344 (2013).
8. Berry, R., Jeffery, E. & Rodeheffer, M. S. Weighing in on adipocyte precursors. *Cell Metab.* **19**, 8–20 (2014).
9. Slavin, B. G. Fine structural studies on white adipocyte differentiation. *Anat. Rec.* **195**, 63–72 (1979).
10. Berry, R. & Rodeheffer, M. S. Characterization of the adipocyte cellular lineage in vivo. *Nat. Cell Biol.* **15**, 302–308 (2013).
11. Jeffery, E. et al. Characterization of Cre recombinase models for the study of adipose tissue. *Adipocyte* **3**, 206–211 (2014).
12. Cattaneo, P. et al. Parallel lineage-tracing studies establish fibroblasts as the prevailing in vivo adipocyte progenitor. *Cell Rep.* **30**, 571–582.e572 (2020).
13. Tang, Q. Q. & Lane, M. D. Adipogenesis: from stem cell to adipocyte. *Annu. Rev. Biochem.* **81**, 715–736 (2012).
14. Rosen, E. D. & MacDougald, O. A. Adipocyte differentiation from the inside out. *Annu. Rev. Biochem.* **81**, 715–736 (2012).
15. Rodeheffer, M. S., Birsoy, K. & Friedman, J. M. Identification of white adipocyte progenitor cells in vivo. *Cell* **135**, 240–249 (2008).
16. Jeffery, E., Church, C. D., Holtrup, B., Colman, L. & Rodeheffer, M. S. Rapid depot-specific activation of adipocyte precursor cells at the onset of obesity. *Nat. Cell Biol.* **17**, 376–385 (2015).
17. Audano, M. et al. Regulatory mechanisms of the early phase of white adipocyte differentiation: an overview. *Cell. Mol. Life Sci.* **79**, 139 (2022).
18. Mota de Sá, P., Richard, A. J., Hang, H. & Stephens, J. M. Transcriptional regulation of adipogenesis. *Compr. Physiol.* **7**, 635–674 (2017).
19. Ambele, M. A., Dhanraj, P., Giles, R. & Pepper, M. S. Adipogenesis: a complex interplay of multiple molecular determinants and pathways. *Int. J. Mol. Sci.* **21**, 4283 (2020).
20. Audano, M. et al. Zc3h10 regulates adipogenesis by controlling translation and F-actin/mitochondria interaction. *J. Cell Biol.* **220**, e202003173 (2021).
21. Chen, L., Hu, H., Qiu, W., Shi, K. & Kassem, M. Actin depolymerization enhances adipogenic differentiation in human stromal stem cells. *Stem Cell Res.* **29**, 76–83 (2018).
22. Duncan, R. E., Ahmadian, M., Jaworski, K., Sarkadi-Nagy, E. & Sul, H. S. Regulation of lipolysis in adipocytes. *Annu. Rev. Nutr.* **27**, 79–101 (2007).
23. Boucher, J. et al. Differential roles of insulin and IGF-1 receptors in adipose tissue development and function. *Diabetes* **65**, 2201–2213 (2016).
24. Cignarelli, A. et al. Insulin and insulin receptors in adipose tissue development. *Int. J. Mol. Sci.* **20**, 759 (2019).
25. Yuan, Y. et al. Differential roles of insulin receptor in adipocyte progenitor cells in mice. *Mol. Cell. Endocrinol.* **573**, 111968 (2023).
26. Starks, R. D. et al. Regulation of insulin receptor trafficking by Bardet Biedl syndrome proteins. *PLoS Genet.* **11**, e1005311 (2015).
27. Knutson, V. P. Cellular trafficking and processing of the insulin receptor. *FASEB J.* **5**, 2130–2138 (1991).
28. Zhang, X. et al. Homocysteine inhibits pro-insulin receptor cleavage and causes insulin resistance via protein cysteine-homocysteinylation. *Cell Rep.* **37**, 109821 (2021).
29. Zhang, F. et al. cTAGE5/MEA6 plays a critical role in neuronal cellular components trafficking and brain development. *Proc. Natl. Acad. Sci. USA* **115**, E9449–e9458 (2018).
30. Comtesse, N. et al. MGEA6 is tumor-specific overexpressed and frequently recognized by patient-serum antibodies. *Oncogene* **21**, 239–247 (2002).
31. Ma, T., Zhang, F., Wang, Y. & Xu, Z. Molecular mechanisms underlying cTAGE5/MEA6-mediated cargo transport and biological functions. *J. Genet. Genom.* **49**, 519–522 (2022).
32. Santos, A. J., Nogueira, C., Ortega-Bellido, M. & Malhotra, V. TANGO1 and Mia2/cTAGE5 (TALI) cooperate to export bulky pre-chylomicrons/VLDLs from the endoplasmic reticulum. *J. Cell Biol.* **213**, 343–354 (2016).
33. Wang, Y. et al. Mea6 controls VLDL transport through the coordinated regulation of COPII assembly. *Cell Res.* **26**, 787–804 (2016).
34. Ma, T. et al. Ablation of Mea6/cTAGE5 in oligodendrocytes significantly impairs white matter structure and lipid content. *Life Metab.* **2**, 68–80 (2023).
35. Moreno, C. A. et al. Homozygous deletion in MYL9 expands the molecular basis of megacystis-microcolon-intestinal hypoperistalsis syndrome. *Eur. J. Hum. Genet.* **26**, 669–675 (2018).
36. Lv, M., Luo, L. & Chen, X. The landscape of prognostic and immunological role of myosin light chain 9 (MYL9) in human tumors. *Immun. Inflamm. Dis.* **10**, 241–254 (2022).
37. Chen, W. et al. Berardinelli-Seip congenital lipodystrophy 2/seipin is a cell-autonomous regulator of lipolysis essential for adipocyte differentiation. *Mol. Cell. Biol.* **32**, 1099–1111 (2023).
38. Saltiel, A. R. & Kahn, C. R. Insulin signalling and the regulation of glucose and lipid metabolism. *Nature* **414**, 799–806 (2001).
39. Gorden, P., Arakaki, R., Collier, E. & Carpentier, J. L. Biosynthesis and regulation of the insulin receptor. *Yale J. Biol. Med.* **62**, 521–531 (1989).
40. Rödiger, M. et al. Adiponectin release and insulin receptor targeting share trans-Golgi-dependent endosomal trafficking routes. *Mol. Metab.* **8**, 167–179 (2018).
41. Foti, M., Porcheron, G., Fournier, M., Maeder, C. & Carpentier, J. L. The neck of caveolae is a distinct plasma membrane subdomain that concentrates insulin receptors in 3T3-L1 adipocytes. *Proc. Natl. Acad. Sci. USA* **104**, 1242–1247 (2007).
42. Ali, A. T., Hochfeld, W. E., Myburgh, R. & Pepper, M. S. Adipocyte and adipogenesis. *Eur. J. Cell Biol.* **92**, 229–236 (2013).
43. Cristancho, A. G. & Lazar, M. A. Forming functional fat: a growing understanding of adipocyte differentiation. *Nat. Rev. Mol. Cell Biol.* **12**, 722–734 (2011).
44. Zwick, R. K. et al. Adipocyte hypertrophy and lipid dynamics underlie mammary gland remodeling after lactation. *Nat. Commun.* **9**, 3592 (2018).

45. Cortés, V. A. et al. Molecular mechanisms of hepatic steatosis and insulin resistance in the AGPAT2-deficient mouse model of congenital generalized lipodystrophy. *Cell Metab.* **9**, 165–176 (2009).
46. Jun, S. et al. Control of murine brown adipocyte development by GATA6. *Dev. Cell* **58**, 2195–2205.e2195 (2023).
47. Shamsi, F. et al. Vascular smooth muscle-derived Trpv1(+) progenitors are a source of cold-induced thermogenic adipocytes. *Nat. Metab.* **3**, 485–495 (2021).
48. Zhou, W. Y. et al. NR2F6 is essential for brown adipocyte differentiation and systemic metabolic homeostasis. *Mol. Metab.* **81**, 101891 (2024).
49. Du, Q. et al. Generation of mega brown adipose tissue in adults by controlling brown adipocyte differentiation in vivo. *Proc. Natl. Acad. Sci. USA* **119**, e2203307119 (2022).
50. Zhao, G.-N. et al. TMBIM1 is an inhibitor of adipogenesis and its depletion promotes adipocyte hyperplasia and improves obesity-related metabolic disease. *Cell Metab.* **33**, 1640–1654.e1648 (2021).
51. Oguri, Y. et al. CD81 controls beige fat progenitor cell growth and energy balance via FAK signaling. *Cell* **182**, 563–577.e520 (2020).
52. Krendel, M. & Mooseker, M. S. Myosins: tails (and heads) of functional diversity. *Physiology* **20**, 239–251 (2005).
53. Zhang, X. et al. Sustained activation of autophagy suppresses adipocyte maturation via a lipolysis-dependent mechanism. *Autophagy* **16**, 1668–1682 (2020).
54. Zhang, G. et al. The vesicular transporter STX11 governs ATGL-mediated hepatic lipolysis and lipophagy. *iScience* **25**, 104085 (2022).
55. Schott, M. B. et al. Lipid droplet size directs lipolysis and lipophagy catabolism in hepatocytes. *J. Cell Biol.* **218**, 3320–3335 (2019).
56. Zechner, R., Kienesberger, P. C., Haemmerle, G., Zimmermann, R. & Lass, A. Adipose triglyceride lipase and the lipolytic catabolism of cellular fat stores. *J. Lipid Res.* **50**, 3–21 (2009).
57. Cho, C. H., Patel, S. & Rajbhandari, P. Adipose tissue lipid metabolism: lipolysis. *Curr. Opin. Genet. Dev.* **83**, 102114 (2023).
58. Qiao, L., Kinney, B., Schaack, J. & Shao, J. Adiponectin inhibits lipolysis in mouse adipocytes. *Diabetes* **60**, 1519–1527 (2011).
59. Megaloikonomos, P. D. et al. Harvesting, isolation and differentiation of rat adipose-derived stem cells. *Curr. Pharm. Biotechnol.* **19**, 19–29 (2018).
60. Shan, T. et al. Lkb1 controls brown adipose tissue growth and thermogenesis by regulating the intracellular localization of CRTC3. *Nat. Commun.* **7**, 12205 (2016).
61. Love, M. I., Huber, W. & Anders, S. Moderated estimation of fold change and dispersion for RNA-seq data with DESeq2. *Genome Biol.* **15**, 550 (2014).
62. Sinnott-Armstrong, N. et al. Author correction: Genetics of 35 blood and urine biomarkers in the UK Biobank. *Nat. Genet.* **53**, 1622 (2021).
63. Backman, J. D. et al. Exome sequencing and analysis of 454,787 UK Biobank participants. *Nature* **599**, 628–634 (2021).
64. Wang, Y. et al. Genome-wide association study on coordination and agility in 461 Chinese Han males. *Heliyon* **9**, e19268 (2023).

Acknowledgements

We would like to thank Dr. Wanzhu Jin from the Institute of Zoology for providing *Adiponectin-Cre* mice, Dr. Fu-Dong Shi and Dr. Wei-Na Jin from Beijing Tiantan Hospital for providing experimental assistance and editing the manuscript, and Dr. Zhuan Li from Southern Medical University and Ling Yuan from Central South University for their valuable advice. This work was supported by grants from the National Natural Science Foundation of China (82371353).

Author contributions

W.H., Z.X., and J.F. formulated the concept and designed the studies. T.M., X.R., Y.W., and X.Q. performed the experiments. S.C. and Y.W. conducted a Phenome-wide association analysis. K.L. performed the mass spectrometry. Z.C. and D.Z. led bioinformatic analyses. Z.X. and Y.W. provided advice and edited the manuscript. W.H. and J.F. analyzed the data and wrote the manuscript.

Competing interests

The authors declare no competing interests.

Additional information

Supplementary information The online version contains supplementary material available at https://doi.org/10.1038/s41467-025-60698-1.

Correspondence and requests for materials should be addressed to Junwan Fan, Zhiheng Xu or Wenyan He.

Peer review information *Nature Communications* thanks Hiroyuki Nobusue and the other anonymous reviewer(s) for their contribution to the peer review of this work. A peer review file is available.